HHS Public Access

Author manuscript

FASEB J. Author manuscript; available in PMC 2021 January 01.

Published in final edited form as:

FASEB J. 2020 January ; 34(1): 474–493. doi:10.1096/fj.201901174RR.

ROCK2 inhibition enhances the thermogenic program in white and brown fat tissue in mice

Lei Wei[1,2,3], **Michelle Surma**[1], **Yang Yang**[1], **Sarah Tersey**[1,2], **Jianjian Shi**[1]

[1]Herman B Wells Center for Pediatric Research, Department of Pediatrics, Indiana University, School of Medicine, Indianapolis, Indiana, USA.

[2]Center for Diabetes and Metabolic Diseases, Indiana University, School of Medicine, Indianapolis, Indiana, USA.

[3]Department of Cellular and Integrative Physiology, Indiana University, School of Medicine, Indianapolis, Indiana, USA.

Abstract

The RhoA/ROCK-mediated actin cytoskeleton dynamics have been implicated in adipogenesis. The two ROCK isoforms, ROCK1 and ROCK2, are highly homologous. The contribution of ROCK2 to adipogenesis *in vivo* has not been elucidated. The present study aimed at the *in vivo* and *in vitro* roles of ROCK2 in the regulation of adipogenesis and the development of obesity. We performed molecular, histological and metabolic analyses in *ROCK2*$^{+/-}$ and *ROCK2*$^{+/KD}$ mouse models, the latter harboring an allele with a kinase-dead (KD) mutation. Both *ROCK2*$^{+/-}$ and *ROCK2*$^{+/KD}$ mouse models showed a lean body mass phenotype during aging, associated with increased amounts of beige cells in subcutaneous white adipose tissue (sWAT) and increased thermogenic gene expression in all fat depots. *ROCK2*$^{+/-}$ mice on a high-fat diet showed increased energy expenditure accompanying by reduced obesity, and improved insulin sensitivity. *In vitro* differentiated *ROCK2*$^{+/-}$ stromal-vascular (SV) cells revealed increased beige adipogenesis associated with increased thermogenic gene expressions. Treatment with a selective ROCK2 inhibitor, KD025, to inhibit ROCK2 activity in differentiated SV cells reproduced the pro-beige phenotype of *ROCK2*$^{+/-}$ SV cells. In conclusion, ROCK2 activity-mediated actin cytoskeleton dynamics contribute to the inhibition of beige adipogenesis in WAT, and also promotes age-related and diet-induced fat mass gain and insulin resistance.

Keywords

Beige adipogenesis; energy expenditure; obesity; ROCK2; ROCK2-selective inhibitor

Correspondence To: Jianjian Shi, M.D., Herman B Wells Center for Pediatric Research, Department of Pediatrics, Indiana University School of Medicine, 1044 West Walnut Street, R4-240, Indianapolis, IN 46202-5225, Ph: (317) 274-8912, Fax: (317) 278-9298, jishi@iu.edu. Lei Wei, Ph.D., Herman B Wells Center for Pediatric Research, Department of Pediatrics, Indiana University School of Medicine, 1044 West Walnut Street, R4-370, Indianapolis, IN 46202-5225, Ph: (317) 274-7894, Fax: (317) 278-9298, lewei@iu.edu.

Author contributions

J. Shi and L. Wei designed research; J. Shi, M. Surma, Y. Yang, S. Tersey and L. Wei performed research; J. Shi, L. Wei, M. Surma, Y. Yang, and S. Tersey analyzed data; J. Shi and L. Wei wrote the paper.

Conflicts of interest

The authors declare no conflict of interest.

Introduction

Obesity is a major risk factor for the development of type 2 diabetes mellitus and cardiovascular complications (1–3). In 2016, 39% of the world population aged 18 years and over is either overweight or obese (3), and obesity is now one of the most serious concerns to public health. Exploring the pathogeneses involved in the development of obesity and developing novel methods to block excessive body adipose tissue expansion can make a significant impact on public health, for example reducing obesity associated metabolic disorders.

ROCKs are central regulators of the actin cytoskeleton downstream of the small GTPase RhoA (4–6). The two ROCK isoforms, ROCK1 and ROCK2, are highly homologous with 92% amino acid sequence identity in the kinase domain and an overall identity of 65% (4–6). Up-regulated ROCK activity has been involved in the pathogenesis of all aspects of metabolic syndrome including obesity, insulin resistance, dyslipidemia and hypertension (7–10). Studies using ROCK inhibitors in animal models including obesity, diabetes, and associated complications have demonstrated numerous benefits (7, 11, 12). However, because most ROCK inhibitors in these studies are non-isoform selective, systemic treatment results in smooth muscle relaxation and may cause a rapid and obvious drop in blood pressure. The side effects have obviously hampered ROCK inhibition as a novel treatment (13, 14). Isoform-selective inhibition, particularly by a ROCK2 inhibitor that is being currently tested in several clinical trials for non-metabolic diseases showing no major side effects, is emerging as an important breakthrough for systemic treatment (15–17). It thus becomes fundamentally and translationally important to define the functions of ROCK2 in the pathogenesis of metabolic diseases including obesity and insulin resistance.

Genetic approaches have revealed pleiotropic actions of ROCKs in regulating insulin signaling and obesity, the outcome is depending on ROCK isoforms and metabolic organs (8, 18–23). To investigate the direct roles of ROCKs in adipose tissues, ROCK1 was specifically deleted from adipocytes in mice, which showed modest amelioration of insulin sensitivity and insulin signaling, but no significant effects were detected on adipocyte hypertrophy and inflammation under a high-fat diet (HFD) (8), suggesting that the ROCK2 isoform in adipose tissue may play a dominant role in controlling insulin sensitivity and adiposity. Indeed, a partial deletion of ROCK2 in mice on a CD-1 background results in reduced adipocyte hypertrophy associated with reduced production of inflammatory cytokines and insulin resistance (21). Therefore *in vitro* (24) and *in vivo* (7, 8, 21) studies have shown a consistent observation and demonstrated the contributory roles of ROCK2 and RhoA/ROCK activation in adipocytes to the development of insulin resistance. Nevertheless, the role of ROCK2 in adipogenesis and adiposity *in vivo* remains unexplored. ROCK2 deficient mouse embryonic fibroblasts (MEF) show enhanced adipogenesis *in vitro* (24), consistent with other reports indicating that suppression of RhoA/ROCK activity enhances adipocyte differentiation (25–27). However, increased adipogenesis has not been reported in partial ROCK2 deficient mice (21) and in transgenic mice expressing adipocyte-specific dominant-negative RhoA mutant (7). A well-defined role and the underlying mechanism of ROCK2 in adipogenesis need to be elucidated in greater detail. It is important to reconcile

the anti-adipogenic roles of ROCK2 supported by using *in vitro* adipogenesis models with its contributory roles to the development of insulin resistance and obesity observed *in vivo*.

White adipose tissue (WAT) is a main site to store energy in the form of fat, and it is also an important endocrine organ for maintaining metabolic homeostasis (28), whereas brown adipose tissue (BAT) is thermogenic and able to convert glucose and fatty acids to heat, thereby increase energy expenditure. BAT is mainly found in interscapulum in mouse and characterized by constitutively expression of high levels of thermogenic genes, notably uncoupling protein-1 (UCP1), a mitochondrial uncoupling protein (29). UCP1 mediates heat generation in brown adipocytes by uncoupling respiratory chain, and thereby manipulating a fast substrate oxidation without efficient ATP production. In addition, clusters of 'brown-like' adipocytes develop in WAT in response to various activators including cold exposure and β-adrenergic stimulation, these cells are also known as UCP1 positive cells or beige cells; it is worthy to note that increased cell activities in either brown or beige adipocytes have been linked to obesity resistance which were reported in numerous studies involving mouse models (28, 30–32) and human (33–38). The new discovery mentioned above suggests that boosting the formation and activation of brown and beige adipocytes holds great promise in metabolic disease therapy.

Increased evidence supports that actin cytoskeleton remodeling plays an important role in brown/beige adipogenesis (31, 39, 40), while the contribution of ROCK isoforms *in vivo* has never been elucidated. In this study, we investigated *in vivo* and *in vitro* roles of ROCK2 in beige adipogenesis, obesity and insulin resistance using both *ROCK2*$^{+/-}$ and *ROCK2*$^{+/KD}$ mouse models, the latter harboring a ROCK2 allele with a kinase-dead (KD) mutation.

Materials and Methods

Cell culture medium and supplement.

Dulbecco's Modified Eagle Medium/Nutrient Mixture F-12 (DMEM/F-12), DMEM, HBSS buffer, Insulin-Transferrin-Selenium-Sodium Pyruvate (ITS-A), 0.4% trypan blue were from Gibco, penicillin/streptomycin mixture (P/S) was from HyClone, fetal bovine serum (FBS) from Atlanta Biologicals, collagenase type II from Worthington Biochemical, indomethacin from Alfa Aesar, D(+)-Biotin from ACROS Organics, 1-methyl-3-isobutylxanthine (IBMX) from Tocris Bioscience, rosiglitazone from AdipoGen Life Science, KD025 (also called SLx-2119) from Apexbio Technology, Y27632 from Millipore-Sigma, Chamber slide for immunocytochemistry from Lab-tek, cell culture dishes and multi-well cell culture plates were purchased from Fisher Scientific.

Experimental mice.

All animal experiments were conducted in accordance with the National Institutes of Health "Guide for the Care and Use of Laboratory Animals" and were approved by the Institutional Animal Care and Use Committee at Indiana University School of Medicine. Generation of *ROCK2*$^{+/-}$ mice on an FVB background was as previously described (41). Deletion of exon 2 in ROCK2 gene results in a frame-shift mutation, removing all residues from the residue 47 to the end of the protein. *ROCK1*$^{+/KD}$ (Fig. S5) and *ROCK2*$^{+/KD}$ (Fig. 5) mice, harboring

a ROCK1 or ROCK2 allele with a KD point-mutation, have been generated in the C57BL/6 background by Merck Research Laboratories (available through Taconic; Rock1 - Model 12904 - PM; Rock2 - Model 12979 - PM). Lysine105 in ROCK1 (Fig. S5A) or Lysine121 in ROCK2 (Fig. 5A), required for ATP binding, has been replaced with Alanine in ROCK1- or ROCK2-KD knockin allele. All animals were housed at 26–28°C with a 12-h light/12-h dark cycle and *ad libitum* access to water and standard pelleted chow (Teklad 2018 SX with 6.2% kcal from fat, Envirgo) or HFD (D12492 with 60% kcal from fat, Research Diets Inc.).

Body composition and food intake.

Mice were weighed at weaning (3 weeks) and weekly thereafter. Total fat and lean mass were assessed using EchoMRI 4in1–500 (EchoMRI). Epididymal WAT (eWAT), inguinal subcutaneous WAT (sWAT), BAT, gastrocnemius muscle, liver and heart were harvested, weighed and immediately frozen in liquid nitrogen for later analysis. To quantitate daily food intake, male and female mice (at 5 month of age) were individually housed, food intake was measured over a 30-day period. To quantitate food intake during HFD feeding, daily food intake was checked over the first 14 days, the time point for mice in two groups to show significant body weight difference.

Blood analyses.

Whole blood was collected from caudal vein of experimental mice; serum was prepared and stored in −80°C freezer until use. Insulin (80-INSMR-CH01), leptin (MOB00), adiponectin (EZMADP-60k) and interleukin 6 (IL-6) (M6000B) were analyzed with The SpectraMax iD5 Multi-Mode Microplate Reader (Molecular Devices, San Jose, CA); alanine aminotransferase (ALT) (AL3875), aspartate aminotransferase (AST) (AS3876) total cholesterol (CH3810), triglyceride (TR3823), high-density lipoprotein (HDL) (CH3811), low-density lipoprotein (LDL) (CH3841) levels were measured with automated clinical chemistry analyzer (The Randox RX Daytona platform). For instant measurement of whole blood total cholesterol, triglyceride, HDL, LDL, the Cholestech LDX Analyzer (Alere) was used.

Glucose and insulin tolerance tests.

All experimental mice were allowed to acclimate to the laboratory environment before study. In the glucose-tolerance tests (GTT), mice were fasted overnight and caudal vein blood glucose was measured using AlphaTrak glucometer immediately before and 10, 20, 30, 60, 90, and 120 min after an intraperitoneal injection of glucose (2.0 g/kg of body weight). In the insulin-tolerance tests (ITT), mice were fasted for 5 h beginning in the morning of experimental day and caudal vein blood was used for glucose level measurement immediately before and 15, 30, 45, and 60 min after an intraperitoneal injection of human insulin (0.75 U/kg of lean body mass; Humulin R, Lilly). Area under the curve was calculated using the trapezoidal rule (18).

Energy expenditure.

Energy expenditure was measured by assessing oxygen consumption and carbon dioxide production with indirect calorimetry. Individually housed mice were studied, using the cages

of TSE systems (Lab Master Metabolic Research Platform). Mice were acclimated in the TSE System cages for 24 h before data collection and had free access to food and water for the duration of the study. Daily oxygen consumption, carbon dioxide production, heat production, locomotor activity and food intake were measured and calculated from the mean of 2 days' values. The respiratory exchange rate (RER) was calculated as the volume of CO_2 versus volume of O_2 (VCO_2/VO_2) ratio. All data were normalized to lean body mass.

Histology and quantitative analysis.

Visceral WAT, inguinal WAT and liver were fixed with 4% paraformaldehyde (4% PFD), embedded in paraffin, sectioned with Leica DM5500B microscope and stained with hematoxylin-eosin (H&E) (Fisher Scientific). Ten representative digital images were taken with a 20× objective from four different sections per animal. Average adipocyte areas of 100–200 cells per animal (4 mice per group) were measured with Image-Pro software (Media Cybernetics). For immunocytochemistry staining, cells were fixed in 4% PFD for 20 min at room temperature, followed by incubation in permeable/block buffer (5% normal goat serum and 0.2% Triton X-100/PBS) for 30 min, then sequential incubation with primary antibodies (UCP1 at 1:500 or p-MLC at 1:50 dilution at 4°C, overnight) and detected with Alexa Fluor 488-conjugated secondary antibody (1:1000 dilution, 1 h at room temperature). Staining for F-actin was with R-415 Rhodamine Phalloidin (1:30 dilution) and for nuclear with Hoechst 33342 (20 mM) (Invitrogen). The fluorescent images were taken with Leica DM5500B microscope (objectives: HCX PL FUOTAR 20.0 × 0.50, HCX PL FUOTAR 40 × 0.75) equipped with a DFC300FXR2 camera, and images were analyzed with the Leica AF6000 software.

Protein analyses.

Protein samples were prepared as previously described (18, 42–46). Fat pads, liver, gastrocnemius muscle and ventricular tissue fragments were disrupted with a PYREX® Potter-Elvehjem tissue grinder on ice in lysis buffer containing proteinase and phosphatase inhibitors (Roche). The homogenate was centrifuged at 15,000 x *g* at 4°C for 15 minutes, and the supernatant was saved for immunoblotting. The blots were probed with primary antibodies to ROCK1 (#sc-5560), ROCK2 (#sc-5561), focal adhesion kinase (FAK) (#sc-558) were purchased from Santa Cruz Biotechnology; ROCK1 (#4035), adiponectin (#2789), acetyl-CoA carboxylase (ACC) (#3676), cytochrome C oxidase subunit IV (COX IV) (#4844), cytochrome C (#4272), CCAAT/enhancer-binding protein α (C/EBPα) (#8178), fatty acid synthase (FAS) (#3180), perilipin (#9349), peroxisome proliferator-activated receptor γ (PPARγ) (#2443), cofilin (#3312), p-cofilin-Ser3 (#3311), p-FAK-Tyr925 (#3284), myosin light chain (MLC) (#3672), p-MLC-Ser19 (#3671), myosin-binding subunit of myosin phosphatase (MYPT) (#2643) were purchased from Cell Signaling Technology; preadipocyte factor 1 (Pref 1) (#AB3511), p-MLC-Ser19 (#AB3381) and p-MYPT-Thr696 (#ABS45) were from MilliporeSigma; UCP1 (#ab10983) from Abcam; p-ROCK2-Ser1366 from GeneTex (GTX122651). All blots were normalized to glyceraldehyde-3-phosphate dehydrogenase (GAPDH) (#ABS16) or actin (#MABT523) obtained from MilliporeSigma.

Insulin signaling analysis.

Insulin signaling studies were performed on mice following overnight fasting as previously performed (8, 18). eWAT, sWAT, BAT, gastrocnemius muscle, liver and heart were harvested 10 min after intraperitoneal injection of human insulin (10 U/kg of body weight), snap-frozen in liquid nitrogen, and stored at −80°C until analysis. Western blot analyses with tissue homogenates were performed with primary antibodies to insulin receptor (IRβ) (#3025), p-IRS1-S632/635 (#2388), Akt (#9272), p-Akt-Ser473 (#9271), and p-Akt-Thr308 (#9275) from Cell Signaling Technology; AMP-activated protein kinase (AMPK) (#07–350), and p-AMPK-Thr172 (#07–681) from MilliporeSigma; p-IRS1-Tyr612 (#44816) and p-IR-Tyr1162/1163 (#44–804) from Invitrogen.

Gene expression analysis.

Total RNA was extracted from eWAT, sWAT, and BAT by using TRIzol™ Reagent (Invitrogen). To assess mRNA transcript levels by real-time quantitative reverse transcription polymerase chain reaction (RT-qPCR), cDNA was synthesized with High-Capacity cDNA Reverse Transcription Kit, TaqMan primers and probes for mouse GAPDH, ROCK1, ROCK2 are from Applied Biosystems; UCP1, PPARγ, elongation of very long chain fatty acids protein 3 (Elovl3), cytochrome C oxidase subunit 8b (COX8b), Resistin, peroxisome proliferator-activated receptor gamma coactivator 1-α (PGC-1α) were from Integrated DNA Technologies. Gene expression was detected with iTq universal SYBR Green in CFX Real-Time PCR Systems from Bio-Rad.

Gene Name	Sequence-F	Sequence-R
UCP1	GCATTCAGAGGCAAATCAGC	GCCACACCTCCAGTCATTAAG
COX8b	GAACCATGAAGCCAACGACT	GCGAAGTTCACAGTGGTTCC
Resistin	CTGTCCAGTCTATCCTTGCACAC	CAGAAGGCACAGCAGTCTTGA
Elovl3	TCCGCGTTCTCATGTAGGTCT	GGACCTGATGCAACCCTATGA
PGC-1α	CACCAAACCCACAGAAAACAG	GGGTCAGAGGAAGAGATAAAGTTG
PPARγ	TTTTCCGAAGAACCATCCGATT	ATGGCATTGTGAGACATCCCC
GAPDH	GTGGAGTCATACTGGAACATGTAG	AATGGTGAAGGTCGGTGTG

Mouse stromal vascular (SV) cells isolation.

WT and ROCK2 gene mutated mice at age 6–8 weeks old were used to prepare SV cells. Before dissecting, the fur of selected mice was disinfected with 70% ethanol spray. All following procedures were performed in an aseptic environment and tissue operations were performed carefully on ice unless indicated otherwise. The isolated fat deposit was placed immediately in a sterile culture dish and weighed in order to determine the volume of digestion buffer (100 mg tissue/400 ul of digestion buffer). The fat deposit was minced quickly in 0.2% collagenase type II in HBSS; minced tissue was then transferred into sterile conic tubes, and further shredded by pipetting up and down with a 5 ml pipette. The enzymatic digestion was carried out at 37°C with constant agitation at 150 rpm for a period of 25–30 min with observations to avoid over-digestion. Tissue homogenate was centrifuged at 700 × g for 10 min at 5°C, the pellet was then re-suspended in DMEM medium and

undigested tissue chucks were cleaned by filtration through Corning sterile 40 – 70 μm cell strainers (Fisher Scientific). The cells were collected by centrifugation at 1200 rpm for 5 min at 5°C in an Allegra 6R centrifuge and were suspended in complete growth medium. The purified SV cells were seeded in culture dishes and maintained at sub-confluence in a humidified atmosphere of 5% CO2 in DMEM supplemented with 10% FBS and 1% P/S at 37°C till 95% cell confluence. For all subsequent experiments, the SV cells with passage number between 1 and 3 were used.

Induction of SV cells differentiation and maintenance.

To induce differentiation, SV cells were cultured in differentiation medium cocktail: DMEM/F-12 with 4% FBS, 10 μg/ml insulin, transferrin 5.5 ug/ml, selenite 6.7 ng/ml, 0.25 mM IBMX, 1 uM dexamethasone, 0.2 mM indomethacin, and 33 μM biotin. The induction period lasted for 48 hours followed by maintaining differentiated cells in medial cocktail: DMEM-F12 (1:1) with 4% FBS, 1 x ITS-A, 0.5 uM dexamethasone, 0.2 mM indomethacin, and 33 μM Biotin. For a subset of experiments, in order to enhance adipogenesis, 0.5 μM rosiglitazone was added. Each specific treatment schedule and drug concentration are indicated in text or figures. In general, the SV cells completed maturation and differentiated to adipocytes in 9 days of our experimental condition. The desired treatment was applied as indicated in text. Cells were collected for protein or RNA analysis as described previously (41, 47); immunocytochemistry analysis was as described previously (41, 47).

Oil Red O (ORO) staining.

ORO (Alfa Aesar) staining is for visualizing accumulated lipid content in cytoplasm of adipocytes. Cell growth in 6-well plates was used for staining. Briefly, ORO was dissolved in isopropanol (3 mg/ml) and diluted with water (3:2 v/v of ORO stock solution and water) before staining. Cells were rinsed once with phosphate buffer saline (PBS) after culture medium was removed and fixed cells in 10% formalin/PBS for 1 hour at RT. Cells were again rinsed with PBS and then 60% isopropanol. Filtered ORO solution (6:4 v/v of stock solution and water) was added and incubated for 15 min at RT. Cells were counter stain with 0.2% trypan blue for 8 min and finally clear background with water.

Statistical analysis.

For cell culture data, all experiments were performed more than three times independently, a representative one was displayed, and all results were presented as means ± SD of at least three independent experiments. Mouse experiments were performed in biological triplicate with at least 4 mice/group for gene/protein expression analyses, with at least 6 mice/group for morphometric and metabolic studies, and all results were expressed as means ± SEM. Comparisons between two groups were performed by Student's *t*-tests using Excel software. For multiple comparisons, one-way or two-way ANOVA was performed using GraphPad Prism 6 software. For all tests, $P < 0.05$ was considered statistically significant.

Results

ROCK2 plays a more important role than ROCK1 in controlling adiposity during the aging process.

ROCK2$^{+/-}$ mice on an FVB background showed reduced body weight (Fig. 1A) and WAT mass (Fig. 1C; Fig. S1A, B) at middle age (10–15 months), compared to WT mice. No significant differences were observed in the amount of food intake (Fig. 1B), or in major organ weights between *ROCK2*$^{+/-}$ and WT groups (Fig. 1D). On the other hand, no significant difference in body weight (Fig. 1A) or WAT mass (Fig. S1C) was observed between *ROCK1*$^{+/-}$ and WT mice, supporting that ROCK2 plays a more important role than ROCK1 in controlling adiposity. Moreover, the fasted serum triglyceride levels were lower in *ROCK2*$^{+/-}$ mice (Fig. 1E), but not in *ROCK1*$^{+/-}$ mice (Fig. S1D). Meanwhile, smaller size of adipocytes was confirmed in eWAT of *ROCK2*$^{+/-}$ mice (Fig. 2A, B). Although there were no significant differences in fasting blood insulin and glucose (Fig. 1G, H) between *ROCK2*$^{+/-}$ and WT groups at 12 months of age, GTT (Fig. 1J) and ITT (Fig. 1L) revealed improved insulin sensitivity in *ROCK2*$^{+/-}$ mice, and the improved GTT and ITT remained at 15 months of age in *ROCK2*$^{+/-}$ mice. In addition, *ROCK2*$^{+/-}$ mice showed an early onset improvement in GTT (Fig. 1I) and ITT (Fig. 1K) at 3 months of age prior to the differences in body weight becoming significant at 10 months of age. Moreover, the improvement of ITT in *ROCK2*$^{+/-}$ mice was more remarkable at 12 months of age than at 3 months of age (Fig. 1K, L), suggesting that age-related improvement of ITT in *ROCK2*$^{+/-}$ mice is connected with the reduced WAT mass.

Partial ROCK2 deletion increases expression of brown adipocyte-selective genes in fat depots.

Brown adipocytes contain multilocular lipid droplets and a high content of mitochondria characterized by uniquely high expression of UCP1 (29). Protein analysis showed increased UCP1, PPARγ, and cytochrome C levels in BAT compared to eWAT and sWAT (Fig. S2A). The levels of common adipocyte markers such as perilipin, ACC, and FAS were similar across fat depots (Fig. S2A). Brown-like or beige adipocytes were also observed interspersed within WAT, particularly enriched in sWAT (Fig. 2C). ROCK2 and total ROCK activity, revealed by p-ROCK2-Ser1366 and/or p-MLC-Ser19 levels, were lowest in BAT and lower in sWAT relative to eWAT (Fig. S2B); there is therefore an inverse relationship between ROCK2 or total ROCK activity and the abundance of brown/beige adipocytes in fat depots. In addition, both ROCK1 and ROCK2 mRNA levels in sWAT were increased during the aging process, but the increased expression ROCK2 gene was higher (Fig. 2D), suggesting that ROCK2 is more likely contributing to suppressing beige adipogenesis.

To determine if ROCK2 is involved in brown/beige cell adipogenesis, we next examined the abundance of multilocular beige adipocytes in sWAT of *ROCK2*$^{+/-}$ mice and also quantitated the adipogenesis markers in BAT and WAT including sWAT and eWAT (Fig. 2E, F). *ROCK2*$^{+/-}$ mice at 12 months, compared to WT mice of the same age, exhibited increased multilocular beige adipocytes in sWAT (Fig. 2C) corresponding to increased UCP1, PPARγ, and cytochrome C protein levels, but no significant changes in perilipin (Fig. 2E, F). In addition, the mRNA levels of thermogenic genes including UCP1, Elovl3, and

Cox8b were elevated in *ROCK2*$^{+/-}$ fat depots at 3 months of age (Fig. 2G), indicating that increased thermogenic gene expression in *ROCK2*$^{+/-}$ fat depots occurs prior to the body weight becoming significantly different at 10 months of age, and likely contributes to the age-dependent lean mass phenotype. Together, these results support a role of ROCK2 in suppressing beige adipogenesis in WAT and in suppressing the thermogenic gene program in both BAT and WAT.

β-adrenergic stimulation has been known for enhancing beige adipocyte formation in sWAT, however, the interplay between ROCK and beige adipocyte formation has never been elucidated in detail, specifically in the context of ROCK isoform. We next examined how *ROCK2*$^{+/-}$ sWAT responded to the β3-adrenergic agonist, CL316,243 (Fig. 2H–K). Mice were treated at 1 mg/kg body weight for 10 days. In both *ROCK2*$^{+/-}$ and WT sWAT, RhoA and ROCK2 levels, and total ROCK activity indicated by p-MLC levels were reduced, but ROCK1 levels were unchanged (Fig. 2H, I; Fig. S2C, D). Due to partial ROCK2 deletion, ROCK2 levels and total ROCK activity (p-MLC levels) were lower in *ROCK2*$^{+/-}$ sWAT, and were further decreased upon CL316,243 treatment relative to WT sWAT (Fig. 2H, I). Parallel to the reduced ROCK2 expression and total ROCK activity, CL316,243 treatment increased the abundance of beige adipocytes (Fig. 2J, K) and the protein levels of thermogenic genes including UCP1 and cytochrome C (Fig. 2H, I) to a greater extent in *ROCK2*$^{+/-}$ sWAT than in WT sWAT, supporting that the *ROCK2*$^{+/-}$ sWAT are more sensitive than the WT sWAT to CL316,243 treatment.

Partial ROCK2 deletion reduces HFD-induced obesity and insulin resistance.

To determine if partial ROCK2 deletion affects the development of adiposity, *ROCK2*$^{+/-}$ mice were fed with HFD for 14 weeks starting from 3 months of age (Fig. 3, Fig. S3). The body weight gain was significantly less in male *ROCK2*$^{+/-}$ mice compared to WT mice after two weeks on HFD (Fig. 3A) while food intake was similar between two groups during 14-week HFD (Fig. 3B, Fig. S3E), and this phenotype has been persistent during the following observation. The WAT mass was significantly less in *ROCK2*$^{+/-}$ mice as measured by EchoMRI after 6 weeks on HFD and by morphometric analysis at the end of diet treatment (Fig. 3C). Moreover, the liver mass was significantly less in *ROCK2*$^{+/-}$ mice (Fig. 3D). Furthermore, body weight, WAT mass and liver mass were reduced in female *ROCK2*$^{+/-}$ mice fed with HFD for 14 weeks (Fig. S3A–D), indicating that *ROCK2*$^{+/-}$ mice are protected against HFD-induced obesity.

Besides, the fasting serum cholesterol (Fig. 3F), HDL (Fig. 3G), leptin (Fig. 3H) and IL-6 (Fig. 3I) levels were lower while serum adiponectin levels (Fig. 3J) were higher in *ROCK2*$^{+/-}$ mice suggesting reduced adipocyte hypertrophy and inflammatory cytokine production in *ROCK2*$^{+/-}$ mice. Interestingly, fasting blood glucose (Fig. 3K) and insulin (Fig. 3L) between *ROCK2*$^{+/-}$ and WT groups did not show significant differences, but both GTT (Fig. 3O) and ITT (Fig. 3P) revealed improved whole body insulin sensitivity in *ROCK2*$^{+/-}$ mice. Finally, liver function in *ROCK2*$^{+/-}$ mice was better than the WT mice as revealed by lower serum ALT (Fig. 3M) and AST (Fig. 3N) levels that are consistent with reduced liver mass (Fig. 3D). In addition, histological analysis revealed reduced hepatic steatosis in *ROCK2*$^{+/-}$ mice (Fig. 3Q). Additional protein analysis with liver homogenates

did not show reduced total ROCK activity (p-MLC and p-cofilin levels) in *ROCK2*$^{+/-}$ liver (Fig. 3R), suggesting that ROCK2 may not be a major contributor of ROCK activity in liver. As there was no significant differences in metabolic signaling molecules (PPARγ, p-AMPK, ACC, cytochrome C) between *ROCK2*$^{+/-}$ and WT liver (Fig. 3R), the reduced hepatic steatosis in *ROCK2*$^{+/-}$ mice is likely attributed to the reduced serum lipid levels (Fig. 3F, G).

β-adrenergic stimulation with CL316,243 significantly reduced body weight in WT mice fed a HFD, but not in *ROCK2*$^{+/-}$ mice fed a HFD (Fig. 4A). Body composition analysis revealed that CL316,243 treatment decreased eWAT and sWAT mass in WT mice (Fig. 4B) consistent with increased beige adipocyte formation and activity by β-adrenergic stimulation. In *ROCK2*$^{+/-}$ mice, CL316,243 treatment increased sWAT and BAT mass while decreasing eWAT mass (Fig. 4B), supporting that the sWAT and BAT of *ROCK2*$^{+/-}$ mice are more sensitive to CL316,243 stimulation and as the result, beige and brown adipocyte formation and activity are increased compared to WT mice.

Metabolic cage analysis following 8 weeks of HFD feeding demonstrated that there was a trend of increased O_2 consumption and heat production in *ROCK2*$^{+/-}$ mice compared to the WT mice; it was about 5% increase during the dark cycle, and the light cycle, or the whole 24-h period (Fig. 4C, D). However, the differences became significant after 10 days of CL316,243 treatment; it was about 5% increase during the light cycle, 15% during the dark cycle, or 10% for the 24-h period (Fig. 4C, D). On the other hand, there were no significant difference in RER (Fig. 4E), locomotor activity (Fig. 4F) and food intake between two groups (Fig. 4G). Body temperature appeared to be elevated in the *ROCK2*$^{+/-}$ group at both baseline and in response to CL316,243 treatment, but the differences were not statistically significant (Figure S3F). The results suggest that higher energy expenditure occurred in *ROCK2*$^{+/-}$ mice. Our observation that CL316,243 treatment increasing the differences of energy expenditure between the two groups is also consistent with the increased sWAT and BAT mass in *ROCK2*$^{+/-}$ mice upon the treatment (Fig. 4B).

Histological and molecular analyses showed that *ROCK2*$^{+/-}$ mice under HFD also exhibited increased multilocular beige adipocytes in sWAT (Fig. S4A) associated with increased thermogenic gene mRNA levels (UCP1, Cox8b, and PGC-1α) and reduced TNFα mRNA levels (Fig. S4B) indicating increased beige adipogenesis and reduced inflammation in *ROCK2*$^{+/-}$ sWAT. In addition, protein analysis showed increased UCP1, PPARγ and cytochrome C protein levels in *ROCK2*$^{+/-}$ sWAT and BAT, and increased PPARγ and cytochrome C protein levels in *ROCK2*$^{+/-}$ eWAT, but no significant changes in perilipin among these fat depots between *ROCK2*$^{+/-}$ and WT mice (Fig. S4C, D). CL316,243 treatment increased the protein expression levels of thermogenic genes including UCP1 and COX IV to a greater extent in *ROCK2*$^{+/-}$ sWAT than in WT sWAT under HFD (Fig. 4H). Therefore, partial ROCK2 deletion stimulated beige adipogenesis in WAT and activated a thermogenic gene program in both BAT and WAT under both HFD feeding (Fig. S4; Fig. 4H) and the aging process (Fig. 2).

Insulin signaling pathway analysis revealed significant increases in p-AKT-Ser473, p-AKT-Thr308 and p-IRS1-Tyr612 levels upon insulin stimulation in the eWAT of *ROCK2*$^{+/-}$ mice compared to that of WT mice, but p-IR-Tyr1162/1163 level among the two groups of mice

was similar and p-IRS1-Ser632/635 level was reduced in the eWAT of *ROCK2*$^{+/-}$ mice (Fig. S4E–G), indicating increased signaling effects downstream of IR activation in the *ROCK2*$^{+/-}$ eWAT. Interestingly, insulin stimulated p-AKT-Ser473 and p-AKT-Thr308 levels were similar in the sWAT of *ROCK2*$^{+/-}$ and WT mice (Fig. S4E, F), suggesting that increased beige adipogenesis in the *ROCK2*$^{+/-}$ sWAT is independent of the response to insulin. Together, these results demonstrates that partial ROCK2 deletion reduces diet-induced obesity and inflammation, increases thermogenic gene program activity in fat depots, and improved WAT and whole body insulin sensitivity.

Inactivating ROCK2 kinase activity reproduces the lean body mass phenotype of partial ROCK2 deletion.

ROCK2 isoform deletion removes both kinase-dependent and independent functions of the ROCK2 protein. To examine the contribution of ROCK2 kinase activity to the age-related fat mass gain, we have extended the study to *ROCK2*$^{+/KD}$ mice (Fig. 5). The *ROCK2*^{KD} allele has recently been generated in the C57BL/6 background by homologous recombination (Fig. 5A). To validate the *ROCK2*^{KD} allele, we first tested if *ROCK2*$^{KD/KD}$ mice are embryonic lethal because homozygous ROCK2 knockout mice are embryonic lethal with placenta dysfunction (~80% penetrance) (48, 49). When the heterozygous ROCK2$^{KD/+}$ mice were intercrossed (>30 crosses), we were unable to obtain any viable *ROCK2*$^{KD/KD}$ mice at weaning age, therefore we have functionally validated this *ROCK2*^{KD} allele during development. In the metabolic study, *ROCK2*$^{+/KD}$ mice reproduced the lean body phenotype of *ROCK2*$^{+/-}$ mice during aging (Fig. 5B) showing reduced body weight (Fig. 5C) and WAT mass (Fig. 5D). The KD point mutation has no detectable effect on ROCK2 protein expression which differs from gene ablation, as ROCK2 expression level was not reduced in sWAT and BAT from *ROCK2*$^{+/KD}$ mice (Fig. 5E, F), but active ROCK2 levels measured by Western blot of p-ROCK2-Ser1366 were reduced by ~50% (Fig. 5E, F). In addition, p-ROCK2 levels were also reduced by ~50% in other tissues of *ROCK2*$^{+/KD}$ mice including eWAT, skeletal muscle, liver, heart and lung without affecting the ROCK2 protein expression (unpublished results). Moreover, reduced total ROCK activity (p-MLC levels) was also observed in the sWAT and BAT of *ROCK2*$^{+/KD}$ mice compared to WT mice. Agreeably with the lean body mass, *ROCK2*$^{+/KD}$ mice exhibited increased UCP1 and cytochrome C protein levels in sWAT and BAT compared to WT mice (Fig. 5E, F), reproducing characteristics of ROCK2 hemizygous mice.

In addition to *ROCK2*$^{+/KD}$ mice, we have characterized *ROCK1*$^{+/KD}$ mice (Fig. S5A), in which ROCK1 kinase activity was reduced in heart homogenates without affecting ROCK1 protein expression levels (Fig. S5B). Additional protein analysis did not show reduced total ROCK activity (p-MLC levels) in *ROCK1*$^{+/KD}$ sWAT and BAT (Fig. S5C), suggesting that ROCK1 is unlikely a major contributor of ROCK activity in fat depots. Similarly to the *ROCK1*$^{+/-}$ mice (Fig. 1A; Fig. S1C), *ROCK1*$^{+/KD}$ mice did not show reduced body weight and fat mass at 12 months of age (Fig. 5C), and did not exhibit increased UCP1 and cytochrome C protein levels in sWAT and BAT compared to WT mice (Fig. S5C). Together, these results further support that ROCK2 plays a more critical role than ROCK1 in regulating body weight, fat mass and beige adipogenesis.

Partial ROCK2 deletion enhances *in vitro* beige adipogenesis.

Because *ROCK2*$^{+/-}$ mice are systemic heterozygous knockout mice, a key question is whether ROCK2 represses beige and brown adipogenesis directly. To address this question, confluent primary SV cells isolated from sWAT of WT and *ROCK2*$^{+/-}$ mice were differentiated *in vitro* by giving signal for differentiation orientation. The cell morphology (Fig. 6A) and protein levels of white and brown adipogenesis markers were examined at day 6 (Fig. 6B, C; Fig. S6A) before reaching maximal levels of differentiation, which occur after day 8. As expected, differentiated SV cells from WT mice showed reduced RhoA protein levels and reduced total ROCK activity (p-MLC and p-cofilin levels) relative to undifferentiated SV cells, accompanied with increased expressions of both common (PPARγ, C/EBPα, perilipin, ACC, FAS) and beige adipocyte (UCP1, cytochrome C, COX IV) markers (Fig. 6A, B). Differentiated *ROCK2*$^{+/-}$ SV cells exhibited smaller lipid droplets compared to the WT cells (Fig. 6A), accompanied with reduced ROCK2 expression and total ROCK activity (p-MLC and p-cofilin levels) (Fig. 6B, C), and increased beige adipogenesis markers (UCP1, cytochrome C, COX IV) and adipogenic transcription factors (PPARγ, C/EBPα). On the other hand, differentiated *ROCK2*$^{+/-}$ SV cells exhibited similar levels of common adipocyte markers, perilipin, ACC and FAS compared to WT cells (Fig. 6B, C). The enhanced beige adipogenesis observed in differentiated *ROCK2*$^{+/-}$ SV cells support a direct action for ROCK2 in suppressing beige adipogenesis.

ROCK2-selective inhibitor (KD025) treatment reduces lipid droplet sizes and increases thermogenic gene expression in differentiated SV cells.

KD025 is a commercially available ROCK2 selective inhibitor, the IC_{50} of this compound was 24 μM for ROCK1 and 0.105 μM for ROCK2 using the recombinant human ROCK1 and ROCK2 proteins (15). We first validated the ROCK2 isoform selectivity of KD025 using ROCK1 or ROCK2 deficient MEF (Fig. S7). KD025 at 10 μM, which is 95-fold of the IC_{50} value of ROCK2, but only 0.42-fold of the IC_{50} value of ROCK1, disrupts actin cytoskeleton in *ROCK1*$^{-/-}$ (only ROCK2 present), but not in *ROCK2*$^{-/-}$ MEFs (absent of ROCK2) and WT MEFs (ROCK1 is able to maintain stress fibers when ROCK2 is inhibited) (Fig. S7A). In addition, phosphorylation of MLC is reduced in KD025 treated WT and *ROCK1*$^{-/-}$ cells (ROCK2 presents in both MEFs) but not in *ROCK2*$^{-/-}$ cells (absent of ROCK2) (Fig. S7B). These results confirm the isoform selectivity of KD025 at 10 μM in cultured cells. Furthermore, the dose curve analysis indicates that KD025 effectively inhibits ROCK2 activity as shown by reduced p-MLC, p-cofilin and p-FAK levels at 5 to 20 μM concentration range in *ROCK1*$^{-/-}$ cells (Fig. S7C).

The preliminary study above defines the conditions for testing effects of KD025 in *in vitro* adipocyte differentiation experiments in which 4 μM of KD025 was used to minimize cytotoxicity while inhibiting ROCK2 activity effectively (Fig. 7). KD025 treatment of confluent primary SV cells reduced endogenous ROCK2 activity and total ROCK activity as indicated by reduced p-ROCK2, p-MLC and p-cofilin levels (Fig. 7A) and reduced central stress fiber formation accompanied by perinuclear re-localization of p-MLC, which mainly associates with central stress fibers in untreated SV cells (Fig. 7B). In addition, KD025 treatment (during the last two days of differentiation) of WT, but not *ROCK2*$^{+/-}$, differentiated SV cells reduced the size of lipid droplet (Fig. 7C), indicating that KD025

treatment reproduced the effects of partial ROCK2 deletion in reducing droplet size. In addition, partial ROCK2 deletion abolished the effects of KD025 (Fig. 7C), supporting the effects of KD025 in reducing the size of lipid droplet are mediated through inhibiting ROCK2.

KD025 treatment increased protein levels of UCP1 and cytochrome C in WT SV cells (Fig. 7D). The pro-beige adipogenic effects of KD025 were further enhanced by co-treatment with rosiglitazone (0.5 μM), a PPARγ agonist knowing to increase both white and beige adipogenesis (Fig. 7D). Different from the differentiated *ROCK2*$^{+/-}$ SV cells (Fig. 6B, C), KD025 treatment reduced perilipin protein levels (Fig. 7D), suggesting inhibition of white adipogenesis by KD025 treatment. In addition, the dose curve analysis showed that KD025 at 0.5 μM, a concentration without significant inhibitory effects on ROCK2 activity (p-ROCK2 levels), effectively inhibited perilipin protein expression (Fig. 7E), suggesting that this anti-adipogenic action of KD025 is not mediated through ROCK2 inhibition. On the other hand, increased UCP1 and cytochrome C expressions could be detected with KD025 treatment at 4 μM, but not at lower concentrations (Fig. 7E), suggesting that KD025 promotes beige adipogenesis through ROCK2 inhibition. In addition, a time course analsyis indicated that in differentiated SV cells, increases in UCP1 and cytochrome C levels could be observed after one day of KD025 treament at 4 μM without signifciant effects on perilipin levels, which decreased during longer treatment period, e.g. from two days of KD025 treatment (Fig. S8A). Consistent with the increased UCP1 levels measured by western blot analysis, fluorescence microscopy analysis revealed increased UCP1 staining in differentiated WT SV cells after one day of KD025 treament at 4 μM (Fig. S8B). Therefore, both dose course and time course analyses dissociated the pro-beige adipogenic effects of KD025 from its anti-adipogenic effects. Moreover, in agreement with the ROCK2 inhibition mediated pro-beige adipogenic effect, the increases in UCP1 and cytochrome C levels were not detected in KD025-treated *ROCK2*$^{+/-}$ SV cells (Fig. S8C). Together, the results indicate that KD025 at optimal concentration can inhibit ROCK2 activity, reduce the size of lipid droplet and increases beige adipocyte markers only in WT SV cells but not in *ROCK2*$^{+/-}$ SV cells. To confirm that the anti-adipogenic effect of KD025 is independent of inhibition of ROCK activity, we treated WT SV cells with Y27632, which inhibits both ROCK1 and ROCK2 (Fig. S7A). Dose curve analysis showed differences between KD025 and Y27632 inhibitions; non-isoform inhibition with Y27632 at 1 to 5 μM increased perilipin levels, therefore promoting adipogenesis (Fig. S8D). Interestingly, Y27632 at 5 μM, not in 1 uM, increased UCP1 and cytochrome C levels (Fig. S8D) indicating that beige adipogenesis rather than white adipogenesis requires efficient disruption of actin cytoskeleton. Together, the results obtained with the cultured SV cells support a model presented in Fig. 8A, in which ROCK2 inhibition, via partial ROCK2 deletion or KD025 treatment (e.g. appropriate concentrations and time frames), facilitates disruption of actin filaments induced by adipogenic factors (see Materials and Methods), and enhances the activation of PPARγ and C/EBPα upon adipogenic induction, resulting in improved beige adipogenesis.

Discussion

The present study revealed a novel role of ROCK2 in promoting the thermogenic program in WAT and BAT through both genetic and chemical inhibition approaches and in both animal

and cell culture experimental models. Importantly, our finding has demonstrated the contribution of ROCK2 activity to age-related fat mass gain and insulin resistance and to HFD-induced obesity and insulin resistance; therefore we have established the role of ROCK2 contributing to obesity and obesity-caused metabolic disease. The most interesting findings in both *ROCK2*$^{+/-}$ and *ROCK2*$^{+/KD}$ mice include: both models exhibiting a lean body mass phenotype during aging when compared to the WT littermates; increased amounts of beige adipocytes in sWAT and augmented thermogenic gene expression in fat depots including eWAT, sWAT and BAT; increased abundance of beige cells and thermogenic gene expression in *ROCK2*$^{+/-}$ mice on HFD; increased sensitivity to β-adrenergic stimulation associated with higher energy expenditure in *ROCK2*$^{+/-}$ mice; reduced obesity and insulin resistance. Besides the above *in vivo* findings, an *in vitro* adipogenesis study on *ROCK2*$^{+/-}$ SV cells has revealed enhanced beige adipogenesis as demonstrated by reduced ROCK activity, reduced the size of lipid droplet and increased thermogenic gene expression. The treatment of differentiated WT SV cells with a ROCK2-selective inhibitor KD025 reproduced the pro-beige adipogenic phenotype of *ROCK2*$^{+/-}$ SV cells. The current study supports the potential therapeutic values of ROCK2-selective inhibitors for the treatment of obesity and insulin resistance.

ROCK2 possesses a preferential role *versus* ROCK1 in controlling beige adipogenesis; we observed that ROCK2 shows a superior role *versus* ROCK1 in controlling actin cytoskeleton dynamics in fat depots (*ROCK2*$^{+/-}$ *versus ROCK1*$^{+/-}$ mice in Fig. 1 and Fig. S1, *ROCK2*$^{+/KD}$ *versus ROCK1*$^{+/KD}$ mice (Fig. 5; Fig. S5). Although previous studies support a negative role of RhoA and ROCK activity in adipogenesis (24–27), a role for this signaling pathway in beige adipogenesis has not been revealed. We indeed found direct evidence to show the role of RhoA and ROCK on adipogenesis *in vivo*, notably in beige adipogenesis. The previously reported genetic manipulations modulate RhoA and ROCK activity either through the upstream regulators (p190-B RhoGAP, RhoGAP DLC1, PDZ-RhoGEF) (25, 26, 39, 50) or downstream mediators [myocardin related transcription factor A (MRTF-A), Yes-associated protein (YAP) and transcriptional co-activator with PDZ-binding motif (TAZ)] (31, 51, 52). The general concept is that RhoA and ROCK activity suppress adipogenesis, which is attributed to acto-myosin generated tension preventing cell shape changes during the differentiation process (24–27). In addition, increased actin stress fiber formation facilitates nuclear translocation of MRTF-A, which is a transcriptional cofactor of serum response factor leading to increased actin cytoskeleton gene expression and decreased PPARγ activity (27). Moreover, RhoA/ROCK-mediated actin cytoskeleton formation also promotes nuclear translocation of transcription factors YAP and TAZ, which promote osteogenesis and suppress adipogenesis (51). Because cell shape change is facilitated by disruption of the actin cytoskeleton, this disruption is required for all white, brown and beige adipocyte differentiation (52); some recent studies indicated that the inhibition of RhoA and ROCK-mediated actin cytoskeleton dynamics is required for all three types of adipogenesis (31, 39, 40). Our observations in this study provide direct support for a negative role of ROCK2 activity in beige adipogenesis *in vivo* and *in vitro*, accordingly linking ROCK2 with previously known RhoA/ROCK upstream and downstream signaling pathways; we therefore further recognize the important metabolic impacts of ROCK2 in obesity. The other result noteworthy is that we found an inverse relationship between ROCK2 activity (and total

ROCK activity) and the abundance of brown/beige adipocytes in fat depots (Fig. 2; Fig. S2), further supports the notion that ROCK2 activity inhibits beige adipogenesis through promoting actin cytoskeleton dynamics.

It is also worth noting that in the previous studies involving the genetic manipulations of RhoA and ROCK, the effects on adipogenesis have not been reported in the partial ROCK2 deficient mice (21), in transgenic mice expressing adipocyte-specific dominant-negative RhoA mutant (7) or in transgenic mice systemically expressing a dominant-negative ROCK mutant inhibiting both ROCK isoforms (12) as these studies are mainly focused on the role of RhoA and ROCK in adipocyte hypertrophy of visceral WAT, insulin resistance and inflammation. Consistent with these studies, we observed that partial ROCK2 deletion is beneficial to amended insulin sensitivity under standard diet at both young (3 months) and middle ages (12 months) (Fig. 1) or under HFD (Fig. 3). An important observation in the current study is that the improved insulin sensitivity measured by ITT in the partial ROCK2 knockout mice at the 3 months of age (Fig. 1K) was further improved at 12 months (Figure 1L), the same beneficial effect was kept when the two mouse groups were challenged with HFD diet (Fig. 3P). In either situation above the reduced WAT gain could be observed in the partial ROCK2 knockout mice (Fig. 1C; Fig. 3C). As the results showed that the insulin sensitivity was improved, we next analyzed insulin signaling molecules and the most noticeable is seen in the eWAT under HFD diet (Fig. S4); supporting that reduced WAT mass in the partial ROCK2 knockout mice most likely contributes to the reduced systemic age-related or diet-related insulin resistance. The results are consistent with a recent study reporting that ROCK activity in rat visceral WAT is important in the development of age-related insulin resistance (53).

An interesting finding in our study is the lean body phenotype observed in the partial ROCK2 knockout mice fed either standard diet during aging or HFD for 14 weeks. This observation differs from recent studies in which partial ROCK2 knockout mice in CD-1 background showed no significant effects on diet-induced body weight gain (20, 21), but showed improved insulin sensitivity under HFD. The discrepancy might be attributed to strain-dependent variations in obesity and glucose homeostasis (54) or to the differences in the experimental time frames. But, in both FVB ($ROCK2^{+/-}$) (Fig. S1A) and C57BL/6 ($ROCK2^{+/KD}$) (Fig. 5B) background, we have observed the lean body mass phenotype with reduced ROCK2 expression or activity during aging, thus further validating the role for ROCK2 activity in adiposity. In addition to fat depots, the liver is also one of the major metabolic organs; thereby the liver may also contribute to the energy expenditure, obesity and insulin sensitivity. We analyzed the liver function and molecules in $ROCK2^{+/-}$ mice; the results showed a reduced hepatic steatosis under HFD (Fig. 3Q) associated with reduced serum ALT (Fig. 3M) and AST (Fig. 3N) levels added onto the benefits of reduced obesity and insulin resistance. A previous report showed that systemically transgenic expression of a dominant-negative ROCK mutant that inhibits both ROCK isoforms increased energy expenditure, reduced diet-induced obesity and insulin resistance through the activation of AMPK in the skeletal muscle and liver (12). However, the contribution of this AMPK-dependent mechanism in liver and skeletal muscle may not play a significant role in the lean body phenotype of $ROCK2^{+/-}$ mice, because we didn't observe an increased AMPK activation (measured by p-AMPK levels) in the liver (Fig. 3R) and skeletal muscle

(unpublished results) of *ROCK2*$^{+/-}$ mice fed HFD, and there were no significant differences in metabolic signaling molecules (PPARγ, p-AMPK, ACC, cytochrome C) between *ROCK2*$^{+/-}$ and WT liver (Fig. 3R). In addition, the liver weight was not increased in the *ROCK2*$^{+/-}$ mice during aging (Fig. 1D), despite of reduced fat mass and improved insulin sensitivity under this condition. Our results support the notion that partial ROCK2 deletion in fat depots mainly contributes to the lean phenotype and improved systemic insulin sensitivity of *ROCK2*$^{+/-}$ mice, and the reduced hepatic steatosis under HFD may be secondary to the reduced serum lipid levels and improved systemic insulin sensitivity. Future studies with conditional ROCK2 deletion in adipose tissue, liver and skeletal muscle are warranted for further validating the metabolic roles of ROCK2 in these tissues.

The underlying mechanisms for ROCK2 inhibiting beige adipogenesis and impairing insulin sensitivity appear to be diverse (Fig. 8). The former involves the ROCK2-mediated actin cytoskeleton dynamics as discussed above (Fig. 8A) and the latter relies on the direct phosphorylation of IRS1 by ROCK2 (Fig. 8B). The relationship between ROCK activity and IRS1 phosphorylation has been documented in various cell types and organs including fat tissues (7, 11, 12, 20, 21, 24, 55–57). It is widely believed that serine phosphorylation of IRS1 by ROCK activity in WAT and vascular cells (11, 20, 21, 24, 55) leads to reduced IRS1-mediated PI3K activation, resulting in decreased insulin sensitivity (Fig. 8B). However, ROCK-mediated IRS1 phosphorylation can also positively impact on insulin signaling such as in skeletal muscle and in cultured adipocytes and muscle cells (18, 19, 56, 57). Therefore, the exact mechanism for ROCK-mediated insulin resistance is not clear yet and multiple crosstalk of ROCK and insulin signaling pathway can occur depending on the cell and tissue context (10). It is also noted that ROCK2-mediated actin cytoskeleton dynamics and insulin signaling can be inter-regulated, therefore the intention to dissociate these two mechanisms is difficult. On one hand, improved insulin signaling observed in the ROCK2 deficient MEFs was linked to increased adipogenesis (24); in contrast, the changes in actin dynamics of ROCK1 deficient MEFs could be linked to improved insulin signaling through increased IR activation (8). It is thus possible that the improved insulin sensitivity in the partial ROCK2 knockout fat tissues may contribute to the enhanced beige adipogenesis. However, our results showed that partial ROCK2 deletion had no significant improvement on insulin signaling in sWAT despite evidence of significantly enhanced beige cell formation, suggesting that the enhanced beige adipogenesis is independent of the effects of partial ROCK2 deletion on insulin signaling. Our results support the model presented in Figure 8B: firstly, ROCK2 activity inhibits beige adipogenesis in sWAT and suppresses the thermogenic gene expressions in all fat depots leading to reduced energy expenditure and increased age-related or diet-induced fat mass gain, specifically the visceral fat mass; secondly, a direct negative action of ROCK2 on insulin signaling; together, age-related or diet-induced insulin resistance is manifest.

Formation of beige adipocytes in WAT could arise by recruiting beige progenitors from perivascular mural cells (58) or from trans-differentiation of mature white adipocytes (59, 60). We have noticed that the expression level of Pref1, a pre-adipocyte marker, was similar between WT and *ROCK2*$^{+/-}$ mice in all fat depots and in cultured primary SV cells (unpublished results) suggesting that ROCK2 may not be involved in the recruitment of progenitors and the expansion of pre-adipocytes. In addition, inhibition of ROCK2 with

KD025 for 2 days after terminal differentiation of SV cells isolated from WT sWAT was able to recapitulate the cellular phenotype of *ROCK2*$^{+/-}$ SV cells, including reduced lipid droplet sizes and increased thermogenic gene expressions (Fig. 7C), raising the possibility that inhibition of ROCK2 could promote trans-differentiation of mature white adipocytes to beige adipocytes under baseline and stimulated conditions (β-adrenergic agonist or PPARγ agonist). Our results also support the notion that the differentiation process of beige and white adipocytes involves down-regulation of RhoA expression and activity by various adipogenic inducers, the latter may suppress actin cytoskeleton formation and acto-myosin contraction. Additional inhibition by ROCK2-selective inhibitor can further reduce total ROCK activity and promotes the adipogenic differentiation towards to beige adipocytes (Fig. 8A).

KD025, published in 2008, is the first highly selective ROCK2-isoform inhibitor (15). Because the hypotensive phenotype that commonly occurred with ROCK pan-inhibitors was not observed when KD025 tested in systemic application (16), it has been emerging as an important breakthrough in systemic application. Indeed, its therapeutic potential has been explored in fibrotic disease (15), focal cerebral ischemia (16, 61, 62) and auto-immune disease (17, 63–66). In addition to the pro-beige adipogenic action of KD025, we have noticed an anti-adipogenic action of KD025 as reflected by reduced perilipin levels in the drug treated SV cells (Fig. 7D, E). Importantly, both dose- and time-dependent analyses (Fig. 7E; Fig. S8A) helped to dissociate the pro-beige adipogenic (mediated by ROCK2 inhibition) and anti-adipogenic (targets are not clear) actions of KD025. Our observations share some similarities with a recent report indicating that treatment of 3T3-L1 cell line with KD025 inhibits adipogenesis, and this anti-adipogenic effect of KD025 is partially independent of ROCK activity (67). However, we have noticed some differences between our study in SV cells with the reported study in 3T3-L1 cells: 1) KD025 treatment reduced total ROCK activity reflected by reduced p-MLC and p-cofilin levels in SV cells, but not 3T3-L1 cells; 2) KD025 treatment disrupted actin cytoskeleton in SV cells, but not 3T3-L1 cells; 3) KD025 reduced adipogenesis on terminally differentiated SV cells, but not on terminally differentiated 3T3-L1 cells; 4) the effects on beige adipogenesis were not examined in 3T3-L1 cells. Further studies are warranted to identify other molecular targets for KD025 implicated in adipogenesis, and to examine if this inhibitor protects against the development of obesity *in vivo* through enhanced beige adipogenesis (through ROCK2 inhibition) and/or reduced white adipogenesis (possibly through other targets).

In conclusion, our study has revealed a preferential role for ROCK2 over ROCK1 in controlling the thermogenic program in fat depots and age-related or diet-induced fat mass gain, and supports the notion that ROCK2 is a potential therapeutic target for the treatment of obesity and insulin resistance. ROCK2 activity-mediated actin cytoskeleton dynamics contribute to the inhibition of beige adipogenesis in WAT and the thermogenic program activity in WAT and BAT. The combined direct action on insulin signaling and an inhibitory effect on adipogenesis by ROCK2 activity promote age-related or diet-induced insulin resistance. Our *in vitro* study in SV cells with ROCK2-selective inhibitor KD025 has demonstrated a pro-beige adipogenesis action through reducing ROCK2 activity and strongly supports our future investigation to explore the therapeutic potential for the treatment of metabolic diseases including obesity and insulin resistance.

Supplementary Material

Refer to Web version on PubMed Central for supplementary material.

Acknowledgments

We thank the Islet and Physiology Core and the Translation Core at Indiana University School of Medicine Center for Diabetes and Metabolic Diseases for their assistance in performing rodent metabolic characterization. We thank Summer Research Interns Maleeka Shrestha, Stephanie Shi, Swati Pant and Dalton Engle for technical help. *ROCK1*$^{+/KD}$ and *ROCK2*$^{+/KD}$ mice were generated in the C57BL/6 background by Merck Research Laboratories (available through Taconic; Rock1 - Model 12904 - PM; Rock2 - Model 12979 - PM).

This work was supported by Biomedical Research Grant of Indiana University School of Medicine 2286128 (to J.S.) awarded from the Indiana Clinical and Translational Sciences Institute (funded in part by grant #UL1 TR001108 from the National Institutes of Health, National Center for Advancing Translational Sciences, Clinical and Translational Sciences) and by the Pilot Funding for Research Use of Core Facilities 2286118 (to J.S.) awarded from the Diabetes Center Core Facilities supported by National Institutes of Health grant P30 DK097512 (to Dr. Raghu G. Mirmira). This work was also supported in part by National Institutes of Health grants HL107537 and HL134599 (to L.W.), and the Riley Children's Foundation (to L.W. and J.S.).

Non-standard Abbreviations:

ACC	acetyl-CoA carboxylase
ALT	alanine aminotransferase
AMPK	AMP-activated protein kinase
AST	aspartate aminotransferase
BAT	brown adipose tissue
C/EBPα	CCAAT/enhancer-binding protein α
Cox8b	cytochrome C oxidase subunit 8b
COX IV	cytochrome C oxidase subunit IV
DMEM	Dulbecco's modified eagle medium
Elovl3	elongation of very long chain fatty acids protein 3
FAK	focal adhesion kinase
FAS	fatty acid synthase
FBS	fetal bovine serum
GAPDH	glyceraldehyde-3-phosphate dehydrogenase
GTT	glucose-tolerance tests
HDL	high-density lipoprotein
H&E	hematoxylin-eosin
HFD	high-fat diet

IBMX	1-methyl-3-isobutylxanthine
IL-6	interleukin 6
IR	insulin receptor
IRS1	insulin receptor substrate 1
ITS-A	insulin-transferrin-selenium-sodium pyruvate
ITT	insulin-tolerance tests
KD	kinase-dead
LDL	low-density lipoprotein
MEF	mouse embryonic fibroblasts
MLC	myosin light chain
MYPT	myosin-binding subunit of myosin phosphatase
ORO	Oil Red O
PBS	phosphate buffer saline
PGC-1α	peroxisome proliferator-activated receptor gamma coactivator 1-α
PFD	paraformaldehyde
PPARγ	peroxisome proliferator-activated receptor γ
Pref1	preadipocyte factor 1
P/S	penicillin/streptomycin mixture
RER	respiratory exchange ratio
RT-qPCR	real-time quantitative reverse transcription polymerase chain reaction
SV	stromal vascular
TNFα	tumor necrosis factor α
UCP1	uncoupling protein 1
WAT	white adipose tissue
eWAT	epididymal WAT
sWAT	subcutaneous WAT

References

1. Inoue Y, Qin B, Poti J, Sokol R, and Gordon-Larsen P (2018) Epidemiology of Obesity in Adults: Latest Trends. Curr Obes Rep 7, 276–288 [PubMed: 30155850]

2. O'Neill S, and O'Driscoll L (2015) Metabolic syndrome: a closer look at the growing epidemic and its associated pathologies. Obes Rev 16, 1–12

3. Organization., W. H. (2019) Fact sheet: obesity and overweight. [WWW document] URL http://www.who.int/mediacentre/factsheets/fs311/en/index.html

4. Matsui T, Amano M, Yamamoto T, Chihara K, Nakafuku M, Ito M, Nakano T, Okawa K, Iwamatsu A, and Kaibuchi K (1996) Rho-associated kinase, a novel serine/threonine kinase, as a putative target for small GTP binding protein Rho. EMBO J 15, 2208–2216 [PubMed: 8641286]

5. Ishizaki T, Maekawa M, Fujisawa K, Okawa K, Iwamatsu A, Fujita A, Watanabe N, Saito Y, Kakizuka A, Morii N, and Narumiya S (1996) The small GTP-binding protein Rho binds to and activates a 160 kDa Ser/Thr protein kinase homologous to myotonic dystrophy kinase. EMBO J 15, 1885–1893 [PubMed: 8617235]

6. Nakagawa O, Fujisawa K, Ishizaki T, Saito Y, Nakao K, and Narumiya S (1996) ROCK-I and ROCK-II, two isoforms of Rho-associated coiled-coil forming protein serine/threonine kinase in mice. FEBS Lett 392, 189–193 [PubMed: 8772201]

7. Hara Y, Wakino S, Tanabe Y, Saito M, Tokuyama H, Washida N, Tatematsu S, Yoshioka K, Homma K, Hasegawa K, Minakuchi H, Fujimura K, Hosoya K, Hayashi K, Nakayama K, and Itoh H (2011) Rho and Rho-kinase activity in adipocytes contributes to a vicious cycle in obesity that may involve mechanical stretch. Sci Signal 4, ra3

8. Lee SH, Huang H, Choi K, Lee DH, Shi J, Liu T, Chun KH, Seo JA, Lima IS, Zabolotny JM, Wei L, and Kim YB (2014) ROCK1 isoform-specific deletion reveals a role for diet-induced insulin resistance. Am J Physiol Endocrinol Metab 306, E332–343 [PubMed: 24326423]

9. Liu L, Tan L, Lai J, Li S, and Wang DW (2016) Enhanced Rho-kinase activity: Pathophysiological relevance in type 2 diabetes. Clin Chim Acta 462, 107–110 [PubMed: 27616626]

10. Jahani V, Kavousi A, Mehri S, and Karimi G (2018) Rho kinase, a potential target in the treatment of metabolic syndrome. Biomed Pharmacother 106, 1024–1030 [PubMed: 30119167]

11. Kanda T, Wakino S, Homma K, Yoshioka K, Tatematsu S, Hasegawa K, Takamatsu I, Sugano N, Hayashi K, and Saruta T (2006) Rho-kinase as a molecular target for insulin resistance and hypertension. FASEB J 20, 169–171 [PubMed: 16267124]

12. Noda K, Nakajima S, Godo S, Saito H, Ikeda S, Shimizu T, Enkhjargal B, Fukumoto Y, Tsukita S, Yamada T, Katagiri H, and Shimokawa H (2014) Rho-kinase inhibition ameliorates metabolic disorders through activation of AMPK pathway in mice. PloS One 9, e110446

13. Feng Y, LoGrasso PV, Defert O, and Li R (2016) Rho Kinase (ROCK) Inhibitors and Their Therapeutic Potential. J Med Chem 59, 2269–2300 [PubMed: 26486225]

14. Defert O, and Boland S (2017) Rho kinase inhibitors: a patent review (2014 – 2016). Expert Opin Ther Pat 27 507–515 [PubMed: 28048944]

15. Boerma M, Fu Q, Wang J, Loose DS, Bartolozzi A, Ellis JL, McGonigle S, Paradise E, Sweetnam P, Fink LM, Vozenin-Brotons MC, and Hauer-Jensen M (2008) Comparative gene expression profiling in three primary human cell lines after treatment with a novel inhibitor of Rho kinase or atorvastatin. Blood Coagul Fibrinolysis 19, 709–718 [PubMed: 18832915]

16. Lee JH, Zheng Y, von Bornstadt D, Wei Y, Balcioglu A, Daneshmand A, Yalcin N, Yu E, Herisson F, Atalay YB, Kim MH, Ahn YJ, Balkaya M, Sweetnam P, Schueller O, Poyurovsky MV, Kim HH, Lo EH, Furie KL, and Ayata C (2014) Selective ROCK2 Inhibition In Focal Cerebral Ischemia. Ann Clin Transl Neurol 1, 2–14 [PubMed: 24466563]

17. Zanin-Zhorov A, Weiss JM, Nyuydzefe MS, Chen W, Scher JU, Mo R, Depoil D, Rao N, Liu B, Wei J, Lucas S, Koslow M, Roche M, Schueller O, Weiss S, Poyurovsky MV, Tonra J, Hippen KL, Dustin ML, Blazar BR, Liu CJ, and Waksal SD (2014) Selective oral ROCK2 inhibitor down-regulates IL-21 and IL-17 secretion in human T cells via STAT3-dependent mechanism. Proc Natl Acad Sci U S A 111, 16814–16819

18. Lee DH, Shi J, Jeoung NH, Kim MS, Zabolotny JM, Lee SW, White MF, Wei L, and Kim YB (2009) Targeted disruption of ROCK1 causes insulin resistance in vivo. J Biol Chem 284, 11776–11780

19. Chun KH, Choi KD, Lee DH, Jung Y, Henry RR, Ciaraldi TP, and Kim YB (2011) In vivo activation of ROCK1 by insulin is impaired in skeletal muscle of humans with type 2 diabetes. Am J Physiol Endocrinol Metab 300, E536–542 [PubMed: 21189360]

20. Soliman H, Nyamandi V, Garcia-Patino M, Varela JN, Bankar G, Lin G, Jia Z, and MacLeod KM (2015) Partial deletion of ROCK2 protects mice from high-fat diet-induced cardiac insulin resistance and contractile dysfunction. Am J Physiol Heart Circ Physiol 309, H70–81 [PubMed: 25910808]
21. Soliman H, Varela JN, Nyamandi V, Garcia-Patino M, Lin G, Bankar GR, Jia Z, and MacLeod KM (2016) Attenuation of obesity-induced insulin resistance in mice with heterozygous deletion of ROCK2. Int J Obes (Lond) 40, 1435–1443 [PubMed: 27163743]
22. Zhou X, Li R, Liu X, Wang L, Hui P, Chan L, Saha PK, and Hu Z (2016) ROCK1 reduces mitochondrial content and irisin production in muscle suppressing adipocyte browning and impairing insulin sensitivity. Sci Rep 6, 29669
23. Huang H, Lee SH, Sousa-Lima I, Kim SS, Hwang WM, Dagon Y, Yang WM, Cho S, Kang MC, Seo JA, Shibata M, Cho H, Belew GD, Bhin J, Desai BN, Ryu MJ, Shong M, Li P, Meng H, Chung BH, Hwang D, Kim MS, Park KS, Macedo P, White M, Jones J, and Kim YB (2018) Rho kinase/AMPK axis regulates hepatic lipogenesis during overnutrition. J Clin Invest 128 5335–5350 [PubMed: 30226474]
24. Noguchi M, Hosoda K, Fujikura J, Fujimoto M, Iwakura H, Tomita T, Ishii T, Arai N, Hirata M, Ebihara K, Masuzaki H, Itoh H, Narumiya S, and Nakao K (2007) Genetic and pharmacological inhibition of Rho-associated kinase II enhances adipogenesis. J Biol Chem 282, 29574–29583
25. Sordella R, Jiang W, Chen GC, Curto M, and Settleman J (2003) Modulation of Rho GTPase signaling regulates a switch between adipogenesis and myogenesis. Cell 113, 147–158 [PubMed: 12705864]
26. McBeath R, Pirone DM, Nelson CM, Bhadriraju K, and Chen CS (2004) Cell shape, cytoskeletal tension, and RhoA regulate stem cell lineage commitment. Dev Cell 6, 483–495 [PubMed: 15068789]
27. Nobusue H, Onishi N, Shimizu T, Sugihara E, Oki Y, Sumikawa Y, Chiyoda T, Akashi K, Saya H, and Kano K (2014) Regulation of MKL1 via actin cytoskeleton dynamics drives adipocyte differentiation. Nat Commun 5, 3368 [PubMed: 24569594]
28. Harms M, and Seale P (2013) Brown and beige fat: development, function and therapeutic potential. Nat Med 19, 1252–1263 [PubMed: 24100998]
29. Nedergaard J, Ricquier D, and Kozak LP (2005) Uncoupling proteins: current status and therapeutic prospects. EMBO Rep 6, 917–921 [PubMed: 16179945]
30. Seale P, Conroe HM, Estall J, Kajimura S, Frontini A, Ishibashi J, Cohen P, Cinti S, and Spiegelman BM (2011) Prdm16 determines the thermogenic program of subcutaneous white adipose tissue in mice. J Clin Invest 121, 96–105 [PubMed: 21123942]
31. McDonald ME, Li C, Bian H, Smith BD, Layne MD, and Farmer SR (2015) Myocardin-related transcription factor A regulates conversion of progenitors to beige adipocytes. Cell 160, 105–118 [PubMed: 25579684]
32. Yadav H, Quijano C, Kamaraju AK, Gavrilova O, Malek R, Chen W, Zerfas P, Zhigang D, Wright EC, Stuelten C, Sun P, Lonning S, Skarulis M, Sumner AE, Finkel T, and Rane SG (2011) Protection from obesity and diabetes by blockade of TGF-beta/Smad3 signaling. Cell Metab 14, 67–79 [PubMed: 21723505]
33. Cypess AM, Lehman S, Williams G, Tal I, Rodman D, Goldfine AB, Kuo FC, Palmer EL, Tseng YH, Doria A, Kolodny GM, and Kahn CR (2009) Identification and importance of brown adipose tissue in adult humans. N Engl J Med 360, 1509–1517 [PubMed: 19357406]
34. Saito M, Okamatsu-Ogura Y, Matsushita M, Watanabe K, Yoneshiro T, Nio-Kobayashi J, Iwanaga T, Miyagawa M, Kameya T, Nakada K, Kawai Y, and Tsujisaki M (2009) High incidence of metabolically active brown adipose tissue in healthy adult humans: effects of cold exposure and adiposity. Diabetes 58, 1526–1531 [PubMed: 19401428]
35. van Marken Lichtenbelt WD, Vanhommerig JW, Smulders NM, Drossaerts JM, Kemerink GJ, Bouvy ND, Schrauwen P, and Teule GJ (2009) Cold-activated brown adipose tissue in healthy men. New N Engl J Med 360, 1500–1508
36. Yoneshiro T, Aita S, Matsushita M, Kayahara T, Kameya T, Kawai Y, Iwanaga T, and Saito M (2013) Recruited brown adipose tissue as an antiobesity agent in humans. J Clin Invest 123, 3404–3408 [PubMed: 23867622]

37. Cypess AM, Weiner LS, Roberts-Toler C, Franquet Elia E, Kessler SH, Kahn PA, English J, Chatman K, Trauger SA, Doria A, and Kolodny GM (2015) Activation of human brown adipose tissue by a beta3-adrenergic receptor agonist. Cell Metab 21, 33–38 [PubMed: 25565203]
38. Betz MJ, and Enerback S (2015) Human Brown Adipose Tissue: What We Have Learned So Far. Diabetes 64, 2352–2360 [PubMed: 26050667]
39. Sim CK, Kim SY, Brunmeir R, Zhang Q, Li H, Dharmasegaran D, Leong C, Lim YY, Han W, and Xu F (2017) Regulation of white and brown adipocyte differentiation by RhoGAP DLC1. PloS One 12, e0174761
40. Dorn T, Kornherr J, Parrotta EI, Zawada D, Ayetey H, Santamaria G, Iop L, Mastantuono E, Sinnecker D, Goedel A, Dirschinger RJ, My I, Laue S, Bozoglu T, Baarlink C, Ziegler T, Graf E, Hinkel R, Cuda G, Kaab S, Grace AA, Grosse R, Kupatt C, Meitinger T, Smith AG, Laugwitz KL, and Moretti A (2018) Interplay of cell-cell contacts and RhoA/MRTF-A signaling regulates cardiomyocyte identity. EMBO J 37, e98133
41. Shi J, Wu X, Surma M, Vemula S, Zhang L, Yang Y, Kapur R, and Wei L (2013) Distinct roles for ROCK1 and ROCK2 in the regulation of cell detachment. Cell death & disease 4, e483
42. Shi J, Zhang L, Zhang YW, Surma M, Mark Payne R, and Wei L (2012) Downregulation of doxorubicin-induced myocardial apoptosis accompanies postnatal heart maturation. Am J Physiol Heart Circ Physiol 302, H1603–1613
43. Shi J, Zhang YW, Summers LJ, Dorn GW 2nd, and Wei L (2008) Disruption of ROCK1 gene attenuates cardiac dilation and improves contractile function in pathological cardiac hypertrophy. J Mol Cell Cardiol 44, 551–560 [PubMed: 18178218]
44. Shi J, Zhang YW, Yang Y, Zhang L, and Wei L (2010) ROCK1 plays an essential role in the transition from cardiac hypertrophy to failure in mice. J Mol Cell Cardiol 49, 819–828 [PubMed: 20709073]
45. Shi J, Surma M, and Wei L (2018) Disruption of ROCK1 gene restores autophagic flux and mitigates doxorubicin-induced cardiotoxicity. Oncotarget 9, 12995–13008
46. Shi J, Surma M, Yang Y, and Wei L (2019) Disruption of both ROCK1 and ROCK2 genes in cardiomyocytes promotes autophagy and reduces cardiac fibrosis during aging. FASEB J 33, 7348–7362 [PubMed: 30848941]
47. Surma M, Handy C, Chang J, Kapur R, Wei L, and Shi J (2014) ROCK1 deficiency enhances protective effects of antioxidants against apoptosis and cell detachment. PloS One 9, e90758
48. Thumkeo D, Keel J, Ishizaki T, Hirose M, Nonomura K, Oshima H, Oshima M, Taketo MM, and Narumiya S (2003) Targeted disruption of the mouse rho-associated kinase 2 gene results in intrauterine growth retardation and fetal death. Mol Cell Biol 23, 5043–5055 [PubMed: 12832488]
49. Thumkeo D, Shimizu Y, Sakamoto S, Yamada S, and Narumiya S (2005) ROCK-I and ROCK-II cooperatively regulate closure of eyelid and ventral body wall in mouse embryo. Genes Cells 10, 825–834 [PubMed: 16098146]
50. Chang YJ, Pownall S, Jensen TE, Mouaaz S, Foltz W, Zhou L, Liadis N, Woo M, Hao Z, Dutt P, Bilan PJ, Klip A, Mak T, and Stambolic V (2015) The Rho-guanine nucleotide exchange factor PDZ-RhoGEF governs susceptibility to diet-induced obesity and type 2 diabetes. eLife 4, e06011
51. Dupont S, Morsut L, Aragona M, Enzo E, Giulitti S, Cordenonsi M, Zanconato F, Le Digabel J, Forcato M, Bicciato S, Elvassore N, and Piccolo S (2011) Role of YAP/TAZ in mechanotransduction. Nature 474, 179–183 [PubMed: 21654799]
52. Lin JZ, and Farmer SR (2016) Morphogenetics in brown, beige and white fat development. Adipocyte 5, 130–135 [PubMed: 27386157]
53. Munoz VR, Gaspar RC, Kuga GK, Pavan ICB, Simabuco FM, da Silva ASR, de Moura LP, Cintra DE, Ropelle ER, and Pauli JR (2018) The effects of aging on rho kinase and insulin signalling in skeletal muscle and white adipose tissue of rats. J Gerontol A Biol Sci Med Sci doi: 10.1093/gerona/gly293.
54. Montgomery MK, Hallahan NL, Brown SH, Liu M, Mitchell TW, Cooney GJ, and Turner N (2013) Mouse strain-dependent variation in obesity and glucose homeostasis in response to high-fat feeding. Diabetologia 56, 1129–1139 [PubMed: 23423668]

55. Begum N, Sandu OA, Ito M, Lohmann SM, and Smolenski A (2002) Active Rho kinase (ROK-alpha) associates with insulin receptor substrate-1 and inhibits insulin signaling in vascular smooth muscle cells. J Biol Chem 277, 6214–6222 [PubMed: 11739394]
56. Furukawa N, Ongusaha P, Jahng WJ, Araki K, Choi CS, Kim HJ, Lee YH, Kaibuchi K, Kahn BB, Masuzaki H, Kim JK, Lee SW, and Kim YB (2005) Role of Rho-kinase in regulation of insulin action and glucose homeostasis. Cell Metab 2, 119–129 [PubMed: 16098829]
57. Chun KH, Araki K, Jee Y, Lee DH, Oh BC, Huang H, Park KS, Lee SW, Zabolotny JM, and Kim YB (2012) Regulation of glucose transport by ROCK1 differs from that of ROCK2 and is controlled by actin polymerization. Endocrinology 153, 1649–1662 [PubMed: 22355071]
58. Berry DC, Jiang Y, and Graff JM (2016) Mouse strains to study cold-inducible beige progenitors and beige adipocyte formation and function. Nat Commun 7, 10184
59. Barbatelli G, Murano I, Madsen L, Hao Q, Jimenez M, Kristiansen K, Giacobino JP, De Matteis R, and Cinti S (2010) The emergence of cold-induced brown adipocytes in mouse white fat depots is determined predominantly by white to brown adipocyte transdifferentiation. Am J Physiol Endocrinol Metab 298, E1244–1253
60. Wu J, Bostrom P, Sparks LM, Ye L, Choi JH, Giang AH, Khandekar M, Virtanen KA, Nuutila P, Schaart G, Huang K, Tu H, van Marken Lichtenbelt WD, Hoeks J, Enerback S, Schrauwen P, and Spiegelman BM (2012) Beige adipocytes are a distinct type of thermogenic fat cell in mouse and human. Cell 150, 366–376 [PubMed: 22796012]
61. Akhter M, Qin T, Fischer P, Sadeghian H, Kim HH, Whalen MJ, Goldstein JN, and Ayata C (2018) Rho-kinase inhibitors do not expand hematoma volume in acute experimental intracerebral hemorrhage. Ann Clin Transl Neurol 5, 769–776 [PubMed: 29928660]
62. Sadeghian H, Lacoste B, Qin T, Toussay X, Rosa R, Oka F, Chung DY, Takizawa T, Gu C, and Ayata C (2018) Spreading depolarizations trigger caveolin-1-dependent endothelial transcytosis. Ann Neurol 84, 409–423 [PubMed: 30014540]
63. Flynn R, Paz K, Du J, Reichenbach DK, Taylor PA, Panoskaltsis-Mortari A, Vulic A, Luznik L, MacDonald KK, Hill GR, Nyuydzefe MS, Weiss JM, Chen W, Trzeciak A, Serody JS, Aguilar EG, Murphy WJ, Maillard I, Munn D, Koreth J, Cutler CS, Antin JH, Ritz J, Waksal SD, Zanin-Zhorov A, and Blazar BR (2016) Targeted Rho-associated kinase 2 inhibition suppresses murine and human chronic GVHD through a Stat3-dependent mechanism. Blood 127, 2144–2154 [PubMed: 26983850]
64. Weiss JM, Chen W, Nyuydzefe MS, Trzeciak A, Flynn R, Tonra JR, Marusic S, Blazar BR, Waksal SD, and Zanin-Zhorov A (2016) ROCK2 signaling is required to induce a subset of T follicular helper cells through opposing effects on STATs in autoimmune settings. Sci Signal 9, ra73
65. Zanin-Zhorov A, Flynn R, Waksaland SD, and Blazar BR (2016) Isoform-specific targeting of ROCK proteins in immune cells. Small GTPases 7, 173–177 [PubMed: 27254302]
66. Zanin-Zhorov A, Weiss JM, Trzeciak A, Chen W, Zhang J, Nyuydzefe MS, Arencibia C, Polimera S, Schueller O, Fuentes-Duculan J, Bonifacio KM, Kunjravia N, Cueto I, Soung J, Fleischmann RM, Kivitz A, Lebwohl M, Nunez M, Woodson J, Smith SL, West RF, Berger M, Krueger JG, Ryan JL, and Waksal SD (2017) Cutting Edge: Selective Oral ROCK2 Inhibitor Reduces Clinical Scores in Patients with Psoriasis Vulgaris and Normalizes Skin Pathology via Concurrent Regulation of IL-17 and IL-10. J Immunol 198, 3809–3814 [PubMed: 28389592]
67. Diep DTV, Hong K, Khun T, Zheng M, Ul-Haq A, Jun HS, Kim YB, and Chun KH (2018) Anti-adipogenic effects of KD025 (SLx-2119), a ROCK2-specific inhibitor, in 3T3-L1 cells. Sci Rep 8, 2477 [PubMed: 29410516]

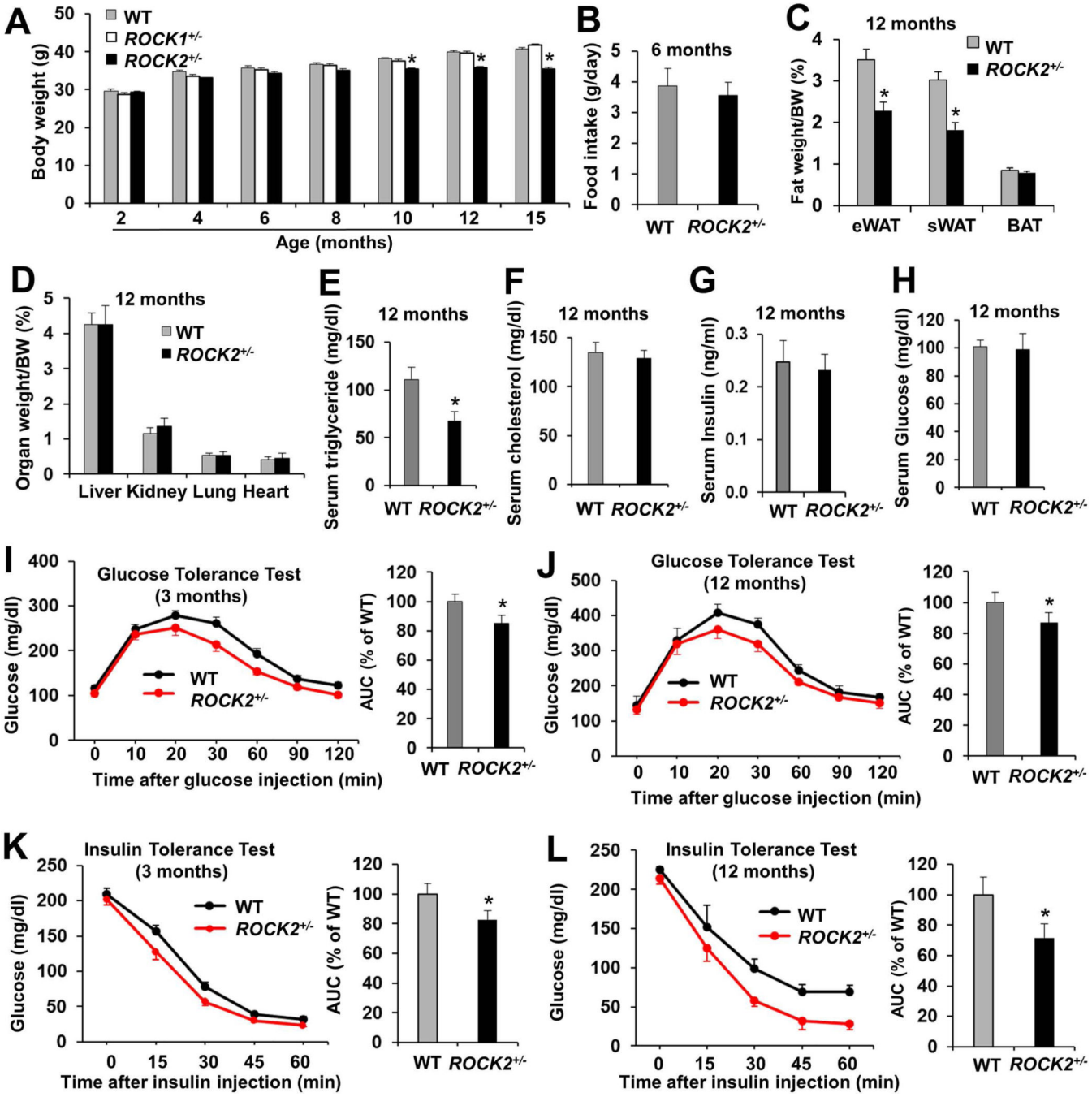

Figure 1. *ROCK2*$^{+/-}$ mice show a lean body mass phenotype and increased insulin sensitivity during the aging process

A. Body weight (males, n = 15–20/group) on standard diet. **B.** Daily food intake prior to the body weight becoming significant different (averaged after 30 days). **C.** Fat depots weight (eWAT, sWAT, BAT) normalized to body weight. **D.** Organ weight normalized to body weight. **E-H**. Metabolic parameters of blood collected from overnight-fasted mice. **I-J.** GTT of overnight fasted mice at 3-month (**I**) and 12-month (**J**) old with IP injection of glucose at 2.0 g/kg of lean body mass. AUC: area under GTT curves. **K-L.** ITT performed in 5 h fasted

mice at 3-month (**K**) and 12-month (**L**) of age, after insulin IP injection at 0.75 U/kg of lean body mass. AUC: area under ITT curves. **B-L:** n = 8–10/group. *$P < 0.05$ *vs.* WT mice.

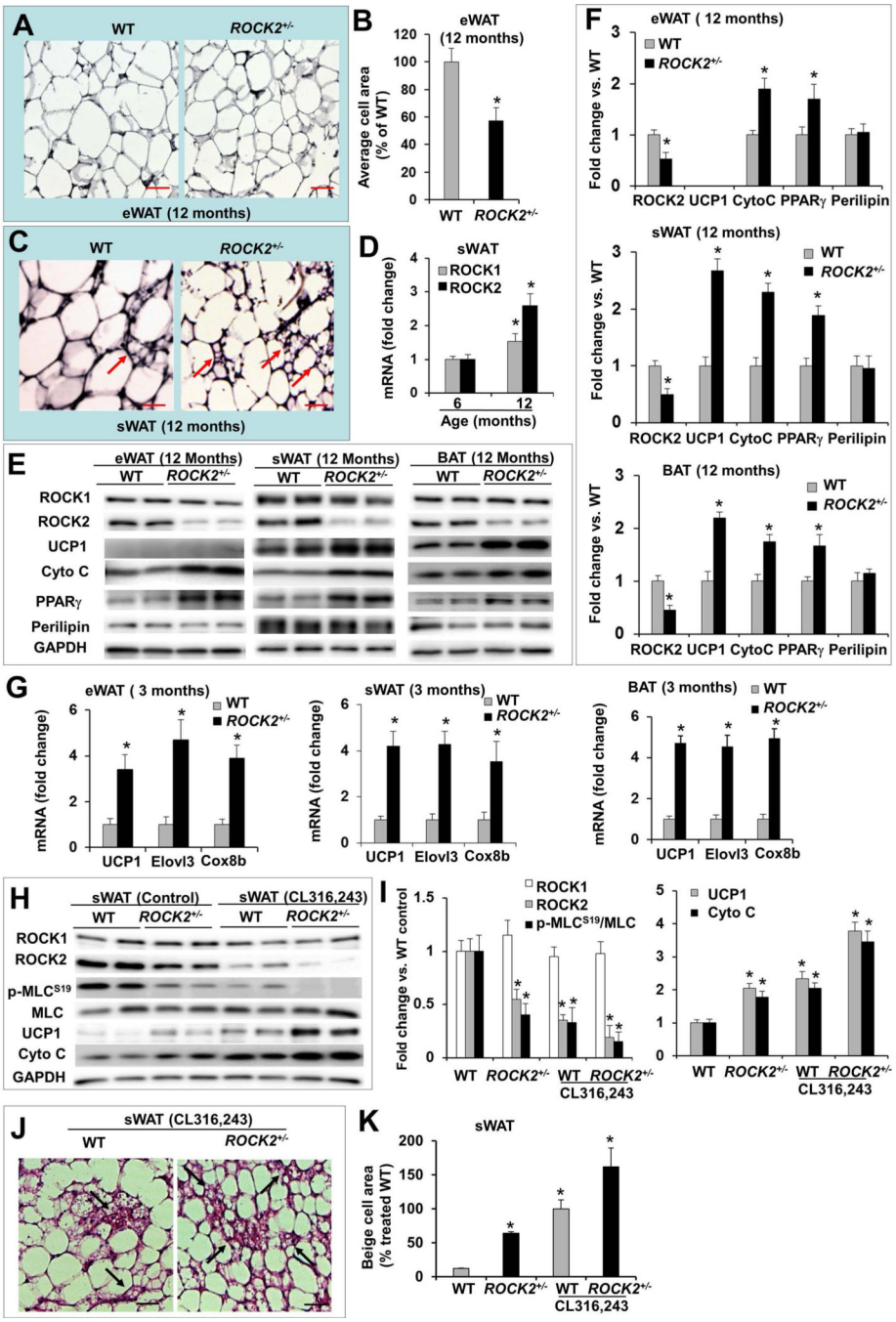

Figure 2. *ROCK2*$^{+/-}$ mice show increased expression of thermogenic genes and higher sensitivity to β-adrenergic signaling attributing to augmentable beige adipocyte formation in subcutaneous fat depots.

A. H&E staining of eWAT from male WT and *ROCK2*$^{+/-}$ mice. **B.** Average adipocyte areas of eWAT, >400 cells from H&E stained sections were measured for each group. **P* < 0.05 *vs.* WT mice. **C.** H&E staining of sWAT (inguinal) (arrows: multilocular beige adipocytes). Bar, 50 μm. **D.** Relative mRNA levels of ROCK1 and ROCK2 in WT sWAT, GAPDH was used as reference gene for this and following quantitative gene expression analysis, the mean normalized value at 6 months was defined as 1.0. **P* < 0.05 *vs.* 6 months. **E-F.**

Representative images (**E**) and quantitative analysis (**F**) of Western blot analysis of eWAT, sWAT and BAT. The expression level of each protein was normalized with GAPDH and the mean normalized value in WT was defined as 1.0. *$P < 0.05$ *vs.* WT mice. **G.** Relative mRNA levels in fat depots of 3-month old mice, the mean normalized value in WT was defined as 1.0. **H-I.** Representative images (**H**) and quantitative analysis (**I**) of Western blot analysis of sWAT. The expression of each protein was normalized to GAPDH level and the mean normalized value in untreated WT was defined as 1.0. n = 4–6/group. *$P < 0.05$ *vs.* untreated WT mice. **J.** H&E staining of paraffin sections of sWAT from 3-month old mice and 10 days post IP injection of CL316,243 (1 mg/kg body weight) showing multilocular beige adipocytes (arrows). Bar, 50 μm. **K.** Quantitative analysis of beige cell area expressed as percent change relative to treated WT mice (n=4–6/group, 5–8 sections/sample). *$P < 0.05$ *vs.* untreated WT mice.

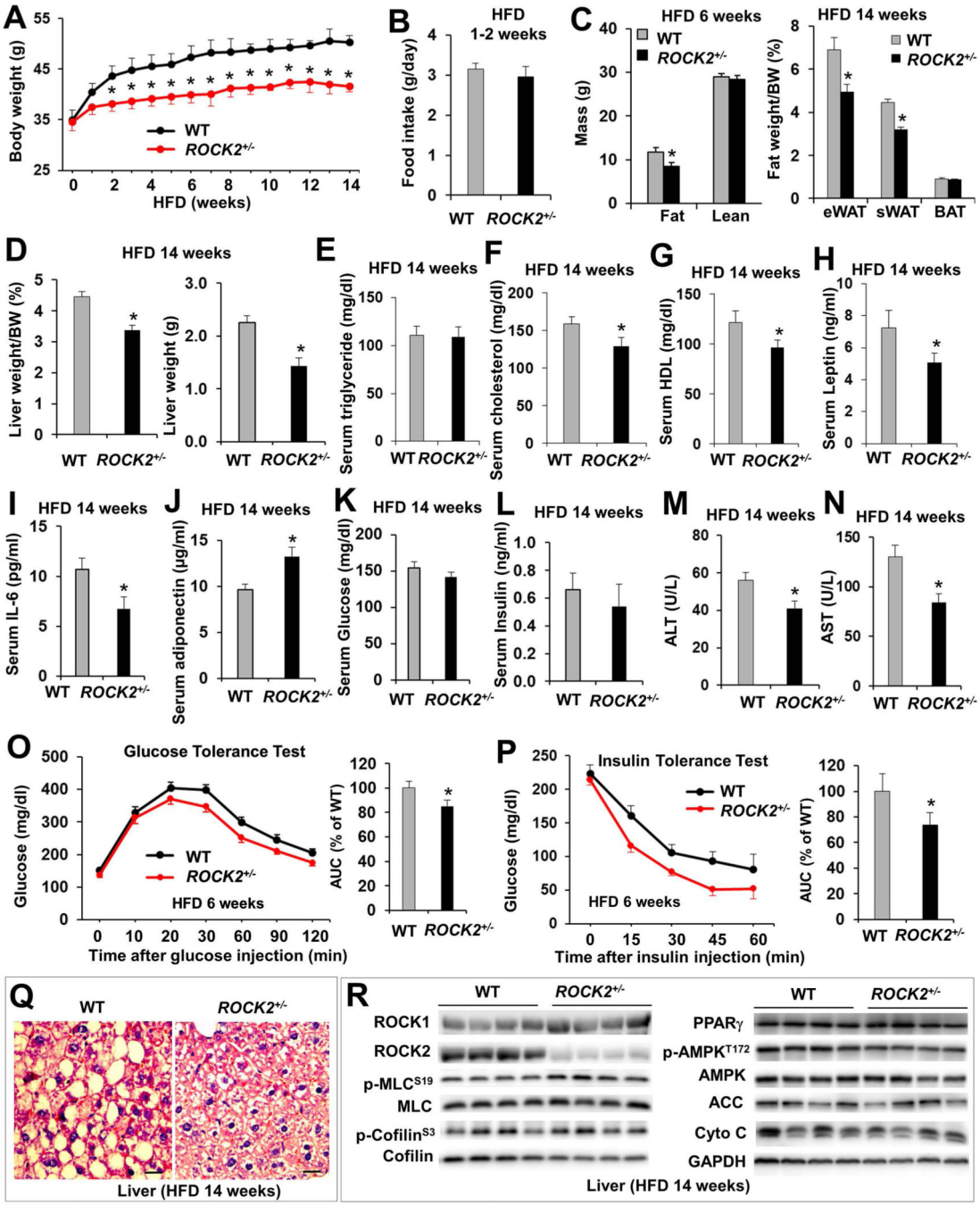

Figure 3. *ROCK2*$^{+/-}$ mice are resistant to HFD induced obesity and insulin resistance, and show reduced hepatic steatosis.

A. Body weight of male mice on a HFD for 14 weeks beginning from 3-month old. **B.** Daily food intake measured during the first two weeks on HFD prior to significant difference in body weight was recorded. **C.** Body composition determined by EchoMRI and fat weights after tissue harvest. **D.** Liver weight. **E-N**. Overnight-fasted metabolic parameters of blood, mice had been on HFD for 14 weeks. **O.** GTT on overnight fasted mice. **P.** ITT on 5 h fasted

mice. **Q.** H&E staining of paraffin sections of liver. Bar, 20 μm. **R.** Representative images of Western blot of liver. **A-P:** n = 8–12/group. *$P < 0.05$ *vs.* WT mice.

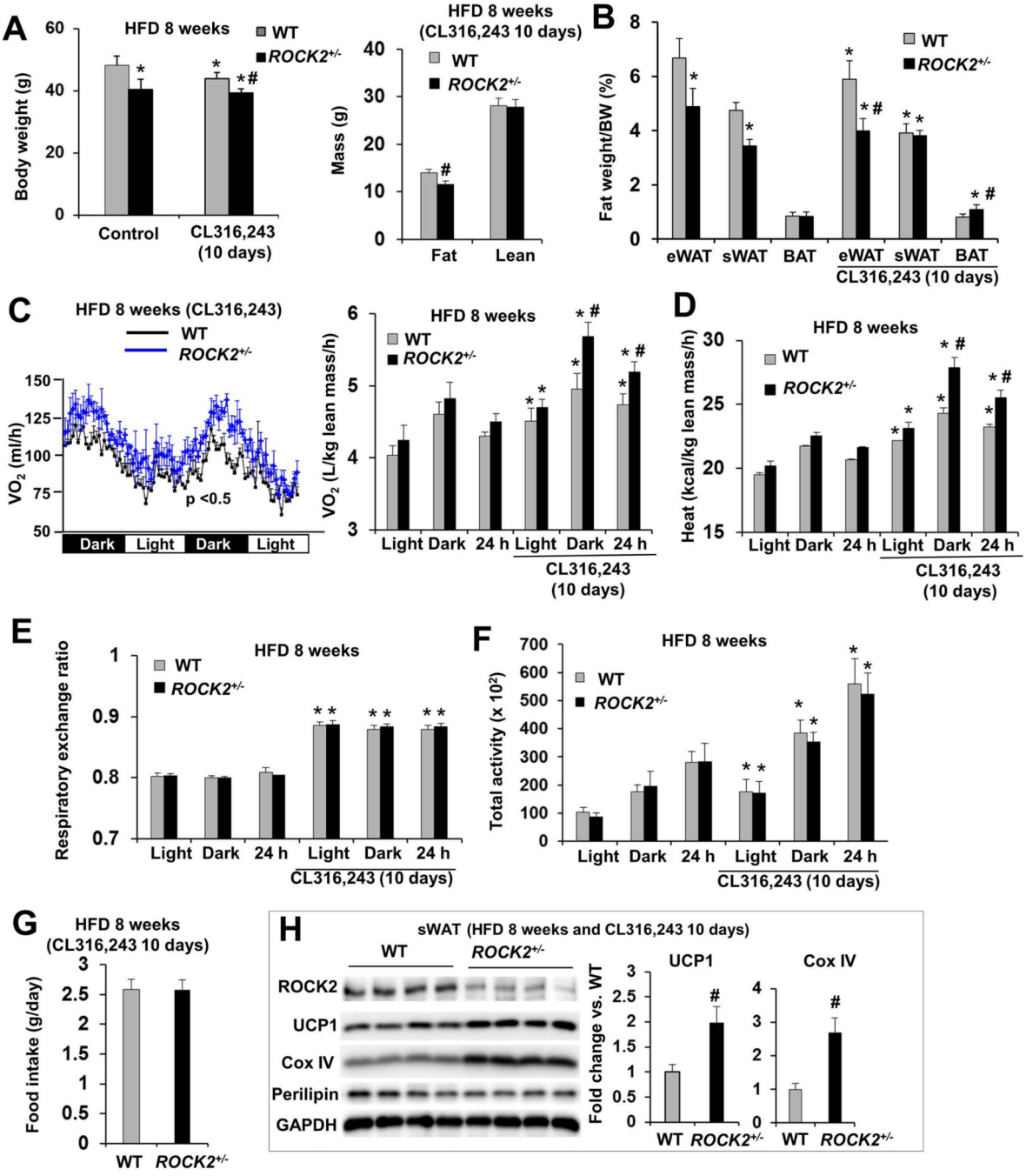

Figure 4. *ROCK2*$^{+/-}$ mice on HFD show increased energy metabolism and expression of thermogenic genes.

A-B. Male mice after 8 weeks of HFD, received or not received the last 10 days of IP injection of CL316,243 (1 mg/kg body weight); body weight (left) and body composition determined by EchoMRI (right) (**A**), fat depots weight (eWAT, sWAT, BAT) normalized to body weight (**B**). **C-G.** Mouse energy expenditure was measured in metabolic cages for two days. O_2 consumption per mouse (left) and normalized to lean body mass (right, the lean body mass is similar between WT and *ROCK2*$^{+/-}$ mice) (**C**), heat production (**D**), RER (**E**),

locomotor activity as the sum of X total and Y total averaged over the dark, light cycle and 24 h (**F**), and food intake (**G**) of male mice in the metabolic cages. **H.** Representative images of Western blot (left) and quantitative analysis of (right) of thermogenic proteins in sWAT of mice treated with CL316,243. **A-H:** n = 6–8/group. *$P < 0.05$ *vs.* untreated WT mice. #$P < 0.05$ *vs.* CL316,243-treated WT mice.

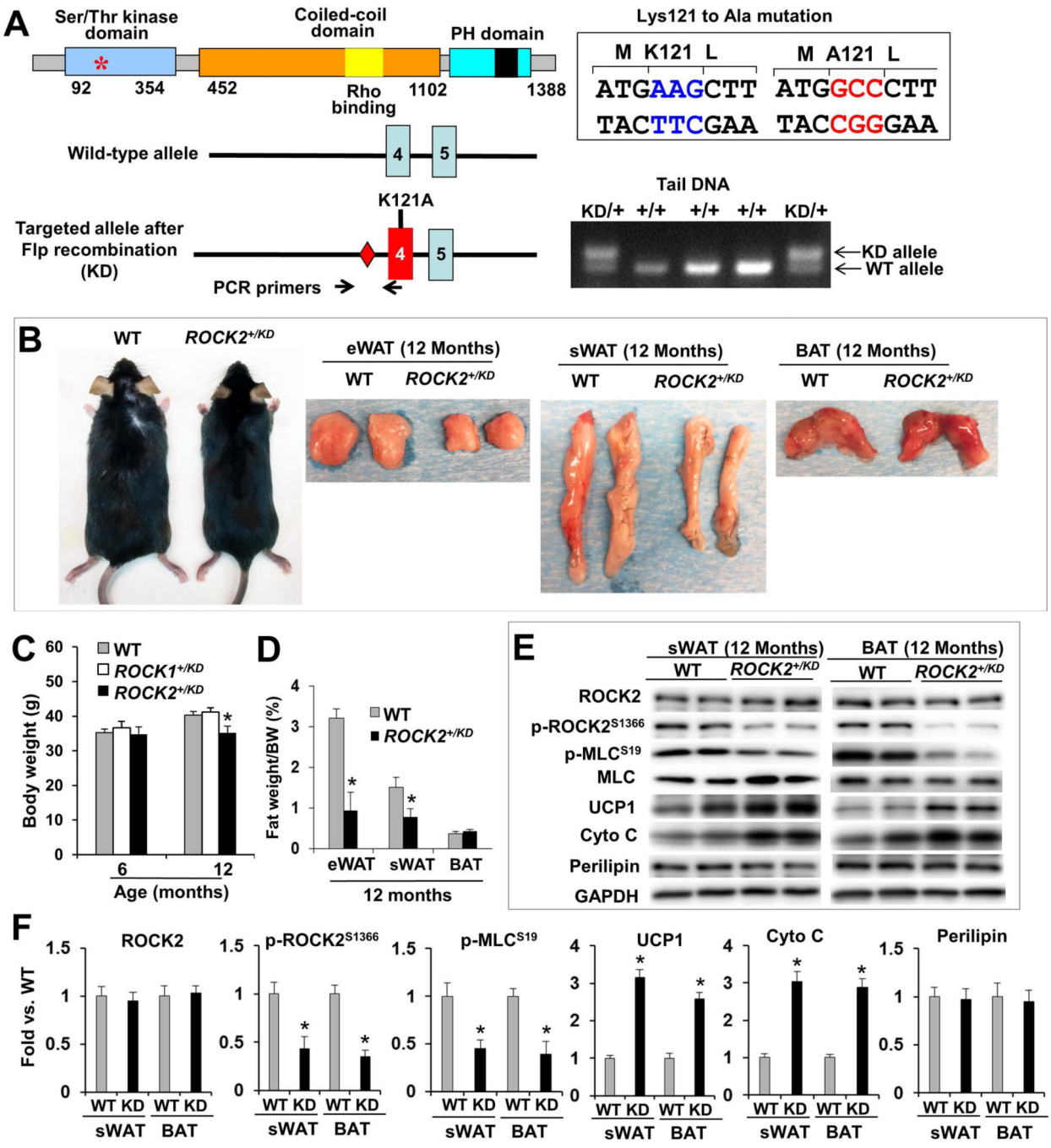

Figure 5. Genetic ROCK2 inactivation reduces body weight and fat mass during aging, associated with increased thermogenic gene expressions.

A. Validation of *ROCK2*$^{+/KD}$ mice. Diagram of ROCK2 protein (top) indicating the position of Lysine121 in the kinase domain, required for ATP binding, which is exchanged with Alanine in ROCK2-KD knockin allele. Diagram of ROCK2-KD allele (bottom), generated by homologous recombination. Diamonds: Frt sites. PCR genotyping with mouse tail DNA at weaning age. The size of the DNA fragment amplified from the KD allele containing the Frt site is larger than that from the WT allele (350 bp vs. 275 bp). **B.** Representative male

WT (left) and *ROCK2*$^{+/KD}$ (right) in C57 background and representative fat depots (eWAT, sWAT, BAT). **C.** Body weight of male WT, *ROCK1*$^{+/KD}$ and *ROCK2*$^{+/KD}$ mice on standard diet. **D.** Fat depots weight normalized to body weight. **E-F:** Representative image of Western blot performed with WT and *ROCK2*$^{+/KD}$ sWAT and BAT **(E)**, and quantitative analysis **(F)**; the KD mutation has no detectable effect on ROCK2 protein levels, but reduces p-ROCK2 (active ROCK2) and p-MLC levels. **C-F:** n = 8/group. $*P < 0.05$ *vs.* WT.

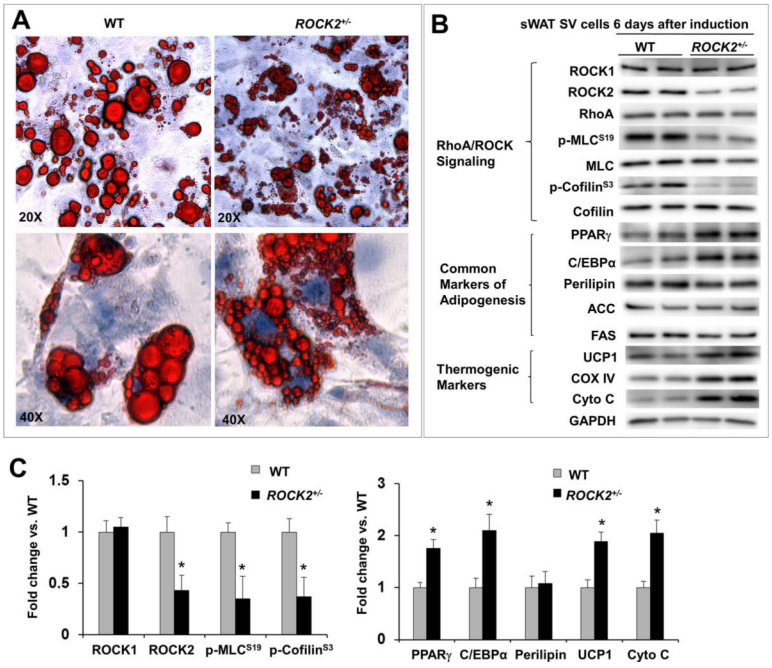

Figure 6. Partial ROCK2 deletion enhances *in vitro* beige adipogenesis.

A. Representative image of ORO staining lipid droplets in SV cells on post differentiation induction day 6, the cells were isolated from sWAT of WT and *ROCK2*$^{+/-}$ mice, showing smaller lipid droplet formations in *ROCK2*$^{+/-}$ cells. **B-C.** Representative images (**B**) and quantitative analysis (**C**) of Western blot analysis of SV cells 6 days post differentiation induction isolated from sWAT of WT and *ROCK2*$^{+/-}$ mice, showing reduced ROCK2 expression and ROCK activity, increased PPARγ and C/EBPα expression, and increased thermogenic protein expression in *ROCK2*$^{+/-}$ cells. The expression level of each protein was normalized to that of GAPDH and the mean normalized value in WT was defined as 1.0 (n = 4–6/group). **P* < 0.05 *vs.* WT mice.

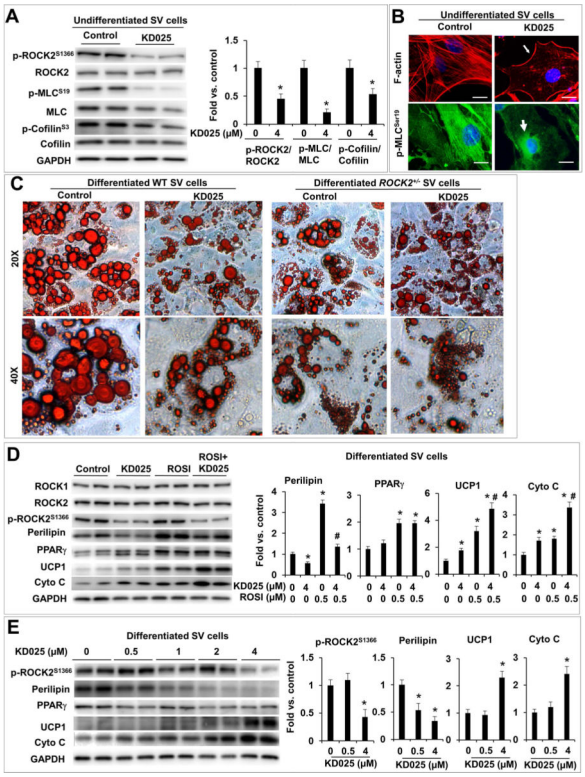

Figure 7. Isoform-specific inhibition of ROCK2 with chemical KD025 enhances *in vitro* beige adipogenesis.

A. Representative images (left) and quantitative analysis (right) of western blot of p-ROCK2, ROCK2, p-MLC, MLC, p-cofilin and cofilin levels in KD025-treated undifferentiated SV cells isolated from sWAT of WT mice. The ratios of p-ROCK2, p-MLC, p-cofilin to ROCK2, MLC and cofilin were expressed as fold change relative to untreated cells. **B.** Phalloidin staining for F-actin (red) and immunostaining of p-MLC (green) showing disruption of central stress fibers, maintaining of peripheral F-actin (thin arrow) and perinuclear localization of p-MLC (thick arrow) in KD025-treated undifferentiated WT SV cells, while p-MLC is co-localized with central stress fibers in untreated cells. Bar, 10 μm. **C.** Representative images of ORO staining lipid droplets accumulated in SV cells from sWAT of WT and *ROCK2*$^{+/-}$ mice 6 days post differentiation induction. KD025 (4 μM) was added for the last 2 days, showing reduced lipid droplet sizes in KD025-treated WT cells, mimicking effects of partial ROCK2 deletion. **D.** Representative images (left) and quantitative analysis (right) of western blot of ROCK1, ROCK2, p-ROCK2, perilipin, PPARγ, UCP1, cytochrome C in differentiated WT SV cells treated with rosiglitazone (ROSI) (0.5 μM) and/or KD025 (4 μM). **E.** Representative images (left) and quantitative analysis (right) of western blot of p-ROCK2, perilipin, PPARγ, UCP1, cytochrome C in differentiated WT SV cells treated with KD025 at indicated concentrations. *$P < 0.05$ *vs.* untreated cells. #$P < 0.05$ *vs.* ROSI-treated cells.

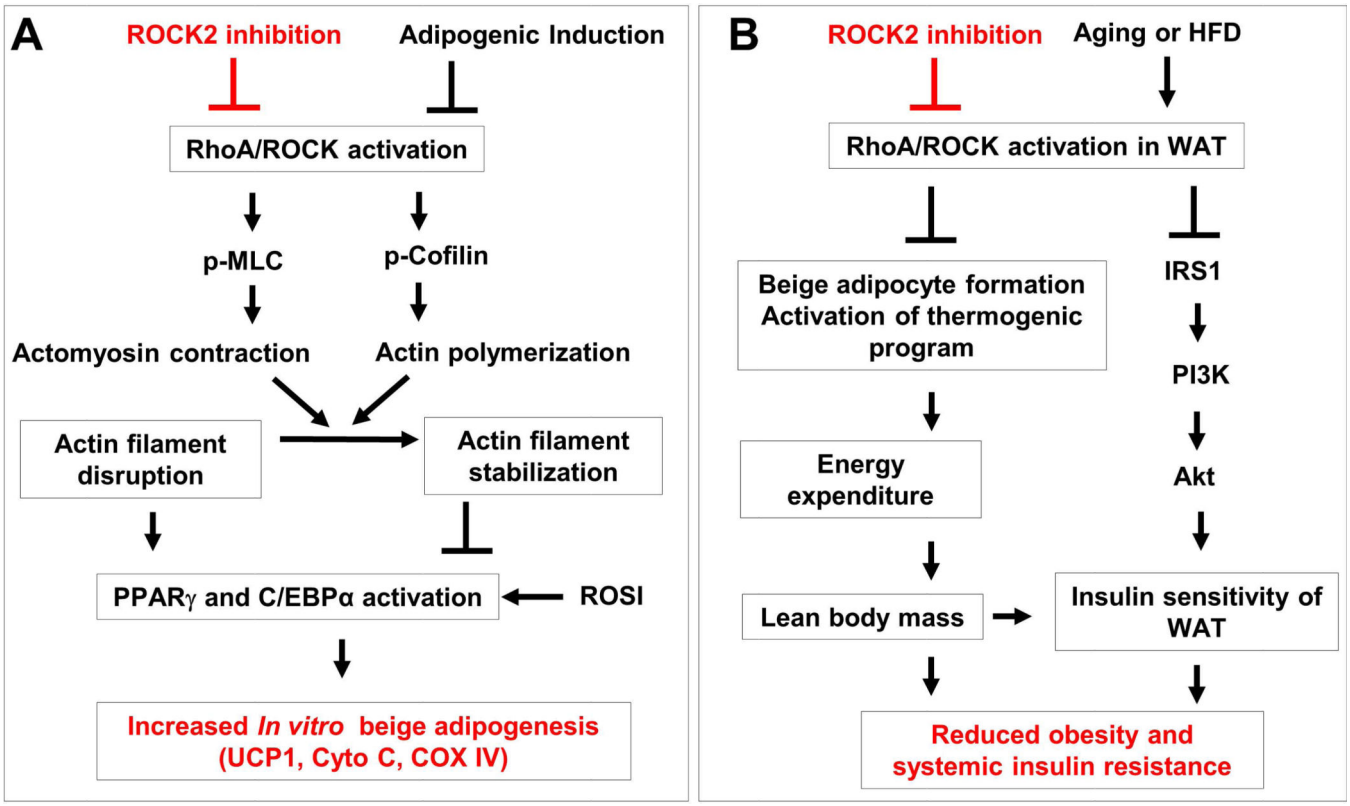

Figure 8. Schematic summary of roles of ROCK2 activity in regulating adipogenesis, obesity and insulin resistance.

A. Model of ROCK2 regulating *in vitro* adipogenesis. ROCK2 inhibition (partial ROCK2 deletion or KD025 treatment) facilitates disruption of actin filaments by adipogenic induction, and enhances the activation of PPARγ and C/EBPα by adipogenic induction, resulting in improved beige adipogenesis. **B.** Schema depicting the actions of ROCK2 inhibition on obesity and insulin resistance. On one hand, ROCK2 inhibition promotes beige adipogenesis in sWAT and activates the thermogenic program in all fat depots leading to increased energy expenditure and reduced fat mass, notably the visceral fat mass. On the other hand, ROCK2 inhibition increases insulin signaling through increased IRS1-mediated PI3K activation, resulting in increased insulin sensitivity, notably in the visceral fat mass. Together, these two positively interacted mechanisms reduce age-related or diet-induced obesity and insulin resistance. Red lines and words indicate the actions of ROCK2 inhibition on beige adipogenesis (**A**) and age-related or diet-induced obesity and insulin resistance (**B**).